

**COMPUTATIONAL MODELING OF REACTING FLOW
INSIDE THE POLYAMIDE 66 POLYMERIZATION LINE**

By

MERT KÜPLÜLÜ

Submitted to the Graduate School of Engineering and
Natural Sciences in partial fulfilment of
the requirements for the degree of Master of Science

Sabancı University

June 2022

THESIS AUTHOR 2022 ©

All Rights Reserved

ABSTRACT

COMPUTATIONAL MODELING OF REACTING FLOW INSIDE THE POLYAMIDE 66 POLYMERIZATION LINE

Mert Küplülü

MFG, M.Sc. Thesis, 2022

Thesis Supervisor: Prof. Dr. Mehmet Yıldız

Keywords: CFD, Comsol, Reacting Flow, Polyamide 66, Polycondensation
Reaction

One of the methods used to manufacture polyamide 66 is continuous polymerization. In this manufacturing process, the reaction proceeds continuously, and a specific viscosity value is reached at the end of the reaction. Degradation and cross-linking may occur due to high temperature with high residence time. The average molecular weight drops, and the viscosity decreases due to degradation. These degradations also affect the viscosity build-up profile estimated along the polymerization line and disturb the viscosity increase homogeneity according to the degradation formation. In this thesis, the effect of the geometric structure of the continuous polymerization line on the viscosity build-up, the viscosity formation profile, and the gel formation were investigated. The reacting flow model was used in the research to analyze the viscosity change and the amount of influence through the nozzle. The temperature-viscosity relationship was established with the curve-fit function and integrated into the COMSOL software with the data obtained from the measurements made in the polymerization line at the Line 1 Nylon Yarn Production Facility Kordsa Teknik Tekstil A.Ş. This temperature-viscosity relation is not given directly for confidentiality reasons, and values have been changed accordingly. Four different nozzle geometry designs were investigated to examine the nozzle geometry effect. First nozzle is designed based on the existing nozzle in

the Kordsa polymerization line, second nozzle is designed with narrow-angle, third nozzle is designed with wide-angle, and fourth nozzle is designed as a straight pipeline. Only the geometry parameters were changed during the analysis by keeping the inlet and outlet boundary conditions and temperature parameters constant. All equation sets and constitutive relations were solved with the assistance of COMSOL software, and analyses were carried out. According to the studies, the viscosity formation profile varied with the change made in the geometry parameters without changing the temperature, inlet, outlet, and wall boundary conditions. In the analyses made in four different nozzles, four different viscosity, temperature, and reaction profiles were obtained. According to the flow analysis, as the pipeline diameter narrows, the polymer in the center heats up more than the wider diameter. However, due to this heating, the reaction dynamics change. In the nozzle, which is designed as a straight pipeline, the reaction rate is the lowest, and the lowest viscosity value is seen. Although the inlet and outlet diameters are identical, obtaining different viscosity formation profiles shows that the diameter contraction angle significantly affects the reaction dynamics.

ÖZET

POLİAMİD 66 POLİMERİZASYON HATTI İÇİ REAKTİF AKIŞIN HESAPLAMALI MODELLENMESİ

Mert Küplülü

MFG, M.Sc. Tezi, 2022

Tez Danışmanı: Prof. Dr. Mehmet Yıldız

Anahtar Kelimeler: Hesaplamalı Akışkanlar Dinamiği, COMSOL, Reaktif Akış,
Polyamide 66

Poliamid 66 üretmek için kullanılan yöntemlerden biri sürekli polimerizasyondur. Bu üretim yönteminde reaksiyon sürekli devam eder ve reaksiyon sonunda ulaşılması hedeflenen belirli bir viskozite değeri vardır. Yüksek sıcaklık veya yüksek bekletme süresi nedenli degradasyon ve çapraz bağlanmalar meydana gelebilir. Bu tezde, sürekli polimerizasyon hattının geometrik yapısının hat çapı üzerindeki viskozite artışına, viskozite oluşum profiline ve jel oluşumuna etkisi araştırılmıştır. Viskozite değişimini ve nozzle boyunca etki miktarını incelemek için reaktif akış modeli analizde kullanılmıştır. Kordsa Teknik Tekstil A.Ş.'nin Hat 1 Naylon İplik Üretim Tesisi'nde bulunan polimerizasyon hattında yapılan ölçümler sonucunda elde edilen verilerle sıcaklık-viskozite ilişkisi curve-fit fonksiyonu ile oluşturulmuş ve COMSOL programına entegre edilmiştir. Gizlilik nedeniyle bu sıcaklık - viskozite ilişkisi doğrudan verilmemiş değerler gizliliği koruyacak şekilde değiştirilmiştir. Nozzle geometri etkisini gözlemlemek için dört farklı nozzle geometri dizaynı analiz edilmiştir. Bu dizaynlar: Kordsa polimerizasyon hattındaki mevcut nozzle baz alınarak tasarlanan nozzle, dar açı ile tasarlanmış nozzle, geniş açı ile tasarlanmış nozzle ve düz boru hattı olarak tasarlanmış nozzle'dır. Analizler sırasında giriş ve çıkış sınır koşulları, sıcaklık parametreleri sabit tutularak yalnızca geometri parametreleri değiştirilmiştir. Tüm denklem setleri ve kurucu ilişkiler Comsol programı yardımı ile çözümlenerek analizler gerçekleştirilmiştir. Yapılan

analizlere göre sıcaklık, giriş, çıkış ve duvar sınır koşullarında herhangi bir değişiklik olmaksızın yalnızca geometride yapılan değişik ile viskozite oluşum profili değişmiştir. Dört farklı nozzleda yapılan analizlerde dört farklı viskozite, sıcaklık ve reaksiyon profili elde edilmiştir. Akış analizine göre boru hattı çapı daraldıkça merkezde bulunan polimer geniş olan hat çapına göre daha çok ısınmaktadır. Bununla birlikte, bu ısıtma nedeniyle reaksiyon dinamikleri değişmektedir. Düz bir boru hattı olarak tasarlanan nozzle tasarımında reaksiyon hızı en düşüktür ve en düşük viskozite değeri bu nozzleda görülmektedir. Giriş ve çıkış hat çapları aynı olmasına rağmen, farklı viskozite oluşum profillerinin elde edilmesi, çap daralma açısının reaksiyon dinamikleri üzerinde önemli bir etkiye sahip olduğunu göstermektedir.

ACKNOWLEDGEMENTS

I would like to express my sincere gratitude to my thesis advisor Prof. Dr. Mehmet Yıldız for giving me the opportunity to work on this project, providing valuable guidance, feedback, and assistance at every stage.

I would like to thank to the thesis committee members Assoc. Prof. Dr. Burcu Saner Okan, PhD and Assist. Prof. Dr. Çağatay Yılmaz for their insightful comments and suggestions.

I would also like to extend my thanks to Suat Hayri Bekircan, İlhan Izmit and Alper Okaygil for all the guidance and support.

Most importantly, I am grateful for my family's unconditional, unequivocal, and loving support.

This thesis is dedicated to my family. For their endless love, support, and encouragement.

TABLE OF CONTENTS

ABSTRACT	4
ÖZET	6
ACKNOWLEDGEMENTS	8
TABLE OF CONTENTS	10
LIST OF TABLES	12
LIST OF FIGURES	13
LIST OF ABBREVIATIONS	14
INTRODUCTION	1
1.1 Motivation.....	1
BACKGROUND	2
2.1. Polycondensation Reaction	2
2.2. Manufacturing of Polyamide 66	3
2.3. Kinetic and Equilibrium Modeling	3
2.4. Nonideal Liquid Model.....	5
2.5. Equilibrium Correlation	6
2.6. Thermal Degradation Kinetics	7
2.7. Molecular Weight and Molecular Weight Distribution	9
FORMULATION OF CFD MODEL	14
3.1. Governing Equations.....	14
3.2. Conservation of Mass.....	14
3.3. Conservation of Momentum	14
3.4. Heat Transfer.....	14
3.5. Chemical Reaction Model.....	15
3.6. CFD Model	16
3.7. Geometry.....	16
3.8. Current Nozzle Design.....	16
3.9. Narrow-Angle Nozzle Design.....	17
3.10. Wide Angle Nozzle Design.....	18
3.11. Straight Line Design	19
3.12. Boundary Conditions	21
3.13. Wall.....	21
3.15. Outlet.....	21
3.16. Wall Temperature Boundary Condition.....	21
3.17. Inflow Heat Boundary Condition.....	21
3.18. Outflow Heat Boundary Condition	22

3.20. Mesh.....	22
CFD PROGRAM VALIDATION ANALYSIS.....	23
4.1. CFD Validation Calculations	23
4.2 Mesh Dependency Analysis.....	24
RESULTS AND DISCUSSION	25
5.1 Case 1 – Current Nozzle Design	25
5.2 Case 2 – Narrow-Angle Nozzle Design.....	28
5.3 Case 3 – Wide-Angle Nozzle Design	30
5.4 Case 4 – Straight Line Design.....	32
5.5 Comparison	34
CONCLUSION	38
FUTURE WORKS.....	39
REFERENCES.....	40

LIST OF TABLES

Table 1 . Parameters for Mark-Houwink Equation.....	12
Table 2 . Design Parameters of the Nozzles	20
Table 3 . Mesh Properties	22
Table 4 . Mesh Size.....	22

LIST OF FIGURES

Figure 1 . Chemical Reaction Curve Fit Graph	15
Figure 2 . Current Design Geometry.....	17
Figure 3 . Narrow-Angle Design Geometry	18
Figure 4 . Wide Angle Design Geometry	19
Figure 5 . Straight Line Geometry	20
Figure 6 . Comparison of theoretically calculated and CFD velocity profiles for a power-law fluid flowing alone: for $V_{in} = 66 \text{ mms} - 1$ ($k = 0.16 \text{ Pa} * \text{sn}, n = 0.81$) and $V_{in} = 33 \text{ mms} - 1$ ($k = 0.75 \text{ Pa} * \text{sn}, n = 0.71$)	24
Figure 7 . Current Design Velocity Profile Contour and Profile	26
Figure 8 . Current Design Isothermal Contour Graph and Temperature Profile Graph	26
Figure 9 . Current Design Viscosity Data Points	27
Figure 10 . Current Design Viscosity Build Up Profile.....	27
Figure 11 . Narrow-Angle Design Velocity Profile Contour and Profile	28
Figure 12 . Narrow-Angle Design Isothermal Contour Graph and Temperature Profile Graph	28
Figure 13 . Narrow-Angle Design Viscosity Data Points.....	29
Figure 14 . Narrow-Angle Design Viscosity Build Up Profile.....	29
Figure 15 . Wide Angle Design Velocity Profile Contour and Profile.....	30
Figure 16 . Wide Angle Design Isothermal Contour Graph and Temperature Profile Graph.....	30
Figure 17 . Wide Angle Design Viscosity Data Points.....	31
Figure 18 . Wide Angle Design Viscosity Build Up Profile.....	31
Figure 19 . Wide Angle Design Velocity Profile Contour and Profile	32
Figure 20 . Straight Line Design Isothermal Contour Graph and Temperature Profile Graph	32
Figure 21 . Straight Line Design Viscosity Data Points	33
Figure 22 . Straight Line Design Viscosity Build Up Profile	33
Figure 23 . Nozzle Outlet Velocity Profile Comparison.....	34
Figure 24 . Polymer Temperature Profile Location	35
Figure 25 . Polymer Temperature Profile for 4 Nozzle Designs	35
Figure 26 . Viscosity Distribution Profile for Four Nozzle Designs Along the Pipe Diameter	36
Figure 27 . Viscosity Build-up Profile for 4 Nozzle Designs Along the Pipe Diameter	37

LIST OF ABBREVIATIONS

CFD

Computational Fluid Dynamics

CHAPTER 1

INTRODUCTION

1.1 Motivation

In the plastic processes, the usage of polyamide is started before the first commercialization of this polymer. The use of polyamides in the industry started by DuPont with the application of Nylon 66 for toothbrush filaments in 1938. [1] Even though the applications of fiber soon dominated, the polyamide usage in the plastics industry expanded progressively since the 1950s, and it was expected to account for more than %25 of total polyamide use in the year 2000. 1.65 million metric tons per year. [2,3]

Polyamides are among the first engineering plastics and prevail to be the most significant and prevalent class of these materials. Their mechanical and thermal properties create a combination that allows them to be used in highly specialized applications and occasionally in metal replacements processes. [4]

Polyamides include a variety of materials, depending on the monomers involved. Polyamide-6,6 and polyamide-6 remain the most common forms, representing more than 90 percent of nylon utilization. The interest in polyamides with higher melting points has increased over the past few years due to high-temperature applications such as the automotive industry and electronic applications. Nylon 4-6 and several semi-automatic nylons were developed depending on the emerging needs. Even though polyamides have excellent thermal stability properties, they tend to degrade when exposed to long hold-up times or high temperatures in the melt form. Degradation cases particularly occur in polyamide, especially in polyamide 66, which contains adipic acid. Chain scission and cyclopentanone production occur due to adipic acid segment cyclization, and carbon dioxide and ammonia release occur at the end of cyclopentanone's chain scission and production. With this degradation, molecular weight loss and cross-linking occur, and the material forms into an interactable gel. When the hold-up or residence time is short, this does not cause any problem. However, molecular weight loss and cross-linking occur due to thermal degradation when the hold-up time is extended. [4]

Considering the above information, this thesis aims to investigate and analyze how the gel formation and molecular weight profile, which are the most crucial continuity parameters of the continuous polymerization line, are affected by the geometric parameters in the line. The nozzles inside the line that enable switching between polymerization equipment were taken as the focus of geometric parameters. The effect on the molecular weight and viscosity profile was examined by changing the geometry parameters of these nozzles.

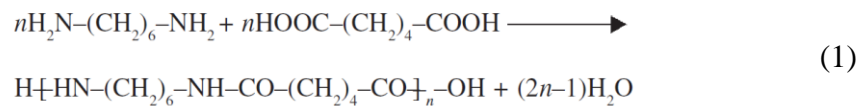
CHAPTER 2

BACKGROUND

2.1. Polycondensation Reaction

There are several ways to produce industrial Nylon 66, and one of the most crucial ways is the polycondensation reaction of diamines and diacids. [5] This reaction method is also included in the process established by Carothers. [6-9] These polymers, composed of diamines and diacids, are generally represented as AABB-type polymers. They are also noted as nylon x, y where x and y represent the carbon atom amount of the reacted diamine and diacid, respectively. Therefore Nylon 66 shows us that there are six atoms of carbon in the diacid and six carbon atoms in the diamine, which are involved in the reaction. [10]

Nylon 66, also known as Polyamide 66, includes hexamethylenediamine in the diacid part and hexandioic acid in the diacid part. These two raw materials produce Nylon 66 with a polycondensation reaction which can also be shown as equation (1).



After starting the polymerization reaction of the polyamides, the polymer's molecular weight or relative molecular mass is one of the essential continuous polymerization control parameters and critical to control. As the molecular weight increase, the viscosity of the polymer also increases. Therefore, the polymer's viscosity and molecular weight are directly linked, and the reaction stage determines these parameters. One of the most important things worth noting is that the molten polymer around the pipe walls moves relatively slowly compared to the whole diameter section of the pipe, causing to degrade and cross-link of the polymer molecules, which end up with the solidification of the polymer inside the pipeline. To have high tenacity, high polymer molecular mass is needed. However, there is a specific molecular mass point, and beyond this point, the tenacity effect of molecular mass is minimal. [11]

To calculate the average molecular mass, which is correlated with the viscosity, the extent of the polymerization, p , is needed to be known. This value p indicates the fraction of the reacted original end groups. As a result, $1-p$ indicates the fraction of the non-reacted end groups. From here, the average degree of polymerization, P_n can be calculated as equation (2). [11]

$$P_n = 1/(1 - p) \quad (2)$$

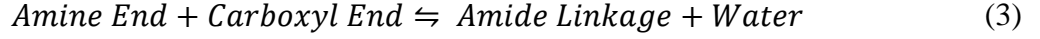
2.2. Manufacturing of Polyamide 66

The polyamide 66 preparation reaction is a polycondensation reaction of hexamethylene diamine and adipic acid. Diamine is prepared as a concentrated aqueous solution, whereas adipic acid is added in a solid form. To start the polymerization reactions of the polyamide 66, its raw material, the salt solution must be prepared according to the specific operating conditions with different controlling points such as concentration, temperature, pH, and salt reactor levels. The concentration is set as %50 - %60, and pH values are critical for regulating the stoichiometric equivalence. The pH value also indicates the distribution of the amine end groups, and even only a 0.1 pH change can change the uniformity of these groups. [10]

After preparing the salt solution, the continuous polymerization phase begins. In this phase, the temperature salt solution is gradually increased, followed by a boiling process at different temperatures depending on the concentration of the solution. After the gradual temperature increase and boiling process, the salt solution is transferred into a reactor where the pressure is set to 250 psi. After a certain hold-up time in this reactor, the polymer molecular weight is achieved at around 4000. After this high-pressure process, the pressure is gradually decreased to trigger the flashing of the water, and eventually, the pressure is decreased to atmospheric, and the flashing of the water is completed. After these stages, the polymer reaction is not in the equilibrium phase. However, the molecular weights become 12000 to 17000. The main goal of these processes is to heat the salt solution gradually and remove water from the medium to move the polymerization reaction forward. While doing this water removal operation, minimum HMD loss should be aimed. The polymerization reaction is limited to the medium's water, steam, and polymer amount at atmospheric pressure. Therefore, specific catalysts should be added to move the reaction forward, and pressure should be reduced more. These catalysts often work in the low water contained medium. The temperature increase is continued in the further processes, and a single-phase reacting flow is obtained in the final stage. This polymer is ready to be sent to the spinning machines through a manifold. [12]

2.3. Kinetic and Equilibrium Modeling

In the preparation of Nylon 66 polymer, four main components are considered to calculate the reaction kinetics. These four components are amine, carboxyl, amide linkage (formed from the reaction of amine and carboxyl), and a water molecule. Amine and Carboxyl groups react and create amide linkage while water molecules are released. This reaction can be represented as [5]



These four components determine the thermodynamic reaction rate and the reaction's equilibrium constants. Therefore, intrinsic reaction rate r can be written as in equation (4):

$$r = k a_A a_C - k' a_L a_W \quad (4)$$

Where k is the forward reaction rate constant and k' is the reverse reaction rate constant. Temperature and a reference state are the only parameters that affect these thermodynamic rates and equilibrium constants. [13]

The apparent equilibrium constant can be written as K_{app} which is formulated as:

$$K_{app} = \frac{x_L x_W}{x_A x_C} \quad (5)$$

The forward reaction rate constant can be written as k_{app} which is formulated as:

$$k_{app} = \frac{r}{x_A x_C - \frac{1}{K_{app} x_L x_W}} \quad (6)$$

x_i represents the mole fraction of the i th component. In the above calculations, mole fractions are preferred instead of concentration values to avoid the density correlation need. Also, these mole fraction values are associated with the reaction activities. The apparent equilibrium constant, thermodynamic rate constant, and equilibrium rate constant relationship can be written as: [13]

$$k_{app} = k \gamma_A \gamma_C \quad (7)$$

Here, γ_A represents the activity coefficient value of material A. Therefore, the apparent equilibrium constant can be defined as:

$$K_{app} = K / K_\gamma \quad (8)$$

$$K_\gamma = \gamma_A \gamma_C / \gamma_L \gamma_W \quad (9)$$

When the solution is ideal, the apparent equilibrium rate, thermodynamic rate, and constants are the same. Nonetheless, when it comes to nonideal solutions, the activity solutions can differ significantly where the apparent rate and equilibrium constants might show a strong

dependence in terms of composition. [13]

Even though it is not a practical approach, the dependence of the apparent rate and the equilibrium constants in terms of composition could be disposed of by doing a sufficient number of trials and experiments in order to identify the relevant species' and side reactions' activities as a function of pressure, temperature, and composition. When just the rate and equilibrium constants are necessary for the reaction calculation, the dependence in terms of composition can be divided into two separate groups, each dependent just on the reactant's activities and the product. Therefore, composition dependence determination is not necessary for each component's activity. [14]

Molecular weight growth in the polyamidation reaction equilibrium is obtained by driving the reaction forward, acquired by removing the water from the medium. The reaction goes forward while removing the water, decreasing the number of polar end groups. This situation dramatically changes the polarity of the reaction medium. Assuming that the end group's molecular size and reactivity are independent, this does not overrule that the end group reactivity is affected by the solution environment. Presently, because the liquid solution is highly nonideal, the equilibria are complicated, and there is an acid catalyst activity inside the polycondensation. There is no applicable chemical model for polyamide polycondensation reaction for an extensive range of variables. [14]

2.4. Nonideal Liquid Model

End groups' polar character and the condensate differ the polyamidation system from ideal solution behavior to nonideal solution behavior along with the activity coefficients, which are far from unity. Below thermodynamic relation shows the temperature relation of the activity coefficient. [15]

$$d \ln \gamma_i = \left(-\frac{\overline{\Delta H}_i}{RT^2} \right) dT \quad (10)$$

Here, $\overline{\Delta H}_i$ is *i*th components' partial molar heat of mixing. For constant pressure and composition, the above equation is strictly accurate. The following apparent rate and equilibrium constant formulas can be obtained by writing the true thermodynamic rate and equilibrium constants using activity parameters. [15]

$$K_{app} = K_0 \exp \left[-\frac{\Delta H_{app}}{R} \left(\frac{1}{T} - \frac{1}{T_0} \right) \right] \quad (11)$$

$$k_{app} = k_0 \exp \left[-\frac{E_{app}}{R} \left(\frac{1}{T} - \frac{1}{T_0} \right) \right] \quad (12)$$

Here, T_0 is an arbitrary reference temperature, $\Delta H_{app} = \overline{\Delta H}_W + \overline{\Delta H}_L - \overline{\Delta H}_A - \overline{\Delta H}_C$ and $E_{app} = -(\overline{\Delta H}_A + \overline{\Delta H}_C)$. When the solution is ideal, the $K_0, k_0, \Delta H_{app}$ and E_{app} are independent in terms of composition however, in this case, they are dependent in terms of mole fractions x_i . Likewise, another exact calculation could be made for k_{app} in case forward and reverse reactions are considered acid-catalyzed. Depending on this consideration, the apparent activation energy can be calculated as $E_{app} = -(\overline{\Delta H}_A + 2\overline{\Delta H}_C)$ and $k_0 = k'_0 x_C$. The nonideal liquid solutions' kinetic models, second and third-order, cannot be separated depending on the existing kinetic data without defining the individual components' activities in the reaction. [15]

2.5. Equilibrium Correlation

Wiloth and Ogata stated that as the water mole fraction ($x_w > 0.2$) increases, and the polyamide 66 polymerization reaction's apparent equilibrium constant decreases. [16-17] Giori and Hayes reported that at %10 or more negligible mole fraction, the apparent equilibrium constant increases as the water contents are increased. At higher water levels, the apparent equilibrium constant is decreased in a way similar to the results that Wiloth and Ogata stated previously for nylon 66. [18] Wiloth also stated that the apparent equilibrium constant increases at extremely low water content. [16] The ratios of methylene, carboxyl, amide, and amine end groups are the same at any transformation for polyamide six and polyamide 66. Therefore, reacting medium's ionic character should be similar to any composition. This indicates that similar equilibrium behavior and reaction rate may be observed for the polyamide 66 system. Jacobs and Zimmerman mentioned that at almost 1 mol% water content, which is considered extremely low, for polyamide 66, equilibrium constant of 250 is found. [19] Another equilibrium constant of 225 is calculated according to Jones and White's presented data. These two values are pretty similar to the equilibrium constant value of 250, which is calculated by Giori and Hayes using the extrapolation technique for polyamide 6 data. These values are also coherent with the widely held lon chain hypothesis. [13]

Ogata addressed High-temperature nylon 6.6 equilibrium applications at low-set water content. These data differ from those of Jacobs and Zimmerman and Jones and White.

Determination of intrinsic polycondensation kinetics can be accomplished more adroitly for thermal sensitive nylon 6,6 related to the data from the comparatively steady nylon 6 structure, and its side reactions have lower complexity amid prolonged high-temperature applications. Nylon 6 comes to equilibrium after around 80 hours at 240°C at a water content of 0.4 water % based on the studies of Wiloth. [16]

2.6. Thermal Degradation Kinetics

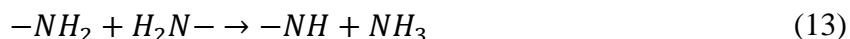
Thermal degradation in polyamide 66 reaction is usually triggered by the adipic acid's remaining sections, which tend to cyclize. After that, because of this cyclization, reactive end groups' balance is changed. This change produces gaseous products of degradation, resulting in chemical changes such as branching, cross-linking, and gelation. [19] These chemical changes caused by unwanted degradation negatively impact the products' ultimate quality, such as processability and physical properties. In order to avoid notable thermal degradation occurrences, several industrial strategies are developed. These strategies enable to decrease the hold-up time of polyamide 66 and increase the molecular weight while avoiding excessive heat up, which can cause thermal degradation. [21]

By complying with rate parameters to the fundamental quantitative data available from the research, Stepan et al. set up a simple kinetic model (referred to as the SDM model) for nylon 66 heat degradation. [13] That would be the single documented model which provides for quantitative estimation and prediction of heat deterioration effects on nylon features under diverse circumstances. For this reason, numerous researchers have adopted the SDM kinetic model by integrating it into their reactor models of different forms of industrial polymerization and processing material. [22]

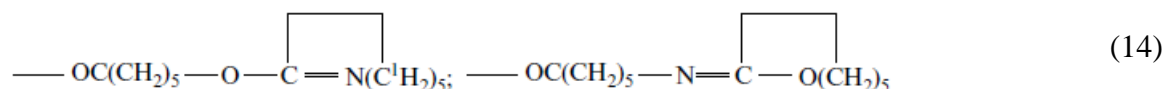
Heat, oxygen, light, and chemical factors are all known to degrade polyamides. Thermal, oxidative, and hydrolytic reactions could be activated throughout melt processing, contributing to the deterioration of features of any produced material in addition to photochemical degradation. The patent literature has detailed several techniques for protecting polyamide fibers from light-induced deterioration. Manganese complexes such as acetates, sulfates, phosphates, and hypophosphates appear successful. The inclusion of copper-I salts and applying antioxidants depending on alkylphenol or aromatic amines in possible conjunction with trialkyl-phenyl phosphates was demonstrated to decrease thermo-oxidative degradation of fibers. [23]

The processing temperatures for polyamide 66 can cause thermal degradation by generating

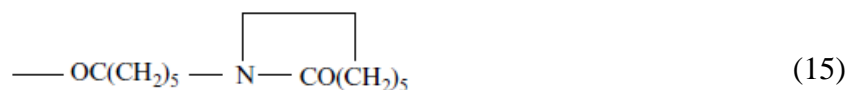
ammonia, carbon dioxide, and water. The reactions of deamination and decarboxylation release ammonia and carbon dioxide; during different reactions of dehydration and condensation release water. Furthermore, amines with low molecular weight, nitriles, and acids can also be created, especially at higher temperatures. [24] Deamination and decarboxylation reactions might occur as side reactions depending on polymerization. As stated below, ammonia is formed by the reaction of two amino end groups. [5]



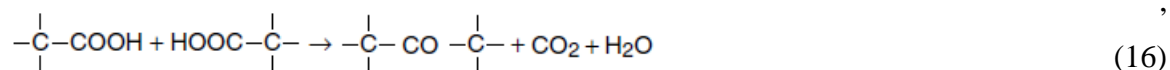
This argument is confirmed by the diamine – diamine separation of highly heat-treated polyamide 6 and polyamide 66 hydrolysis reaction. Nonetheless, it was stated that, for nylon 6, the secondary amine structure quantity was not sufficient for the released amount of ammonia. This indicates that further reactions must be triggering ammonia release. Hence, it was mentioned that one or both of the below imino ether groups might be the reason for the ammonia release. [5]



In this way, it was theorized that ammonia release might be triggered by the production of two imino ether moieties: an amino end group interacting with caprolactam (lactim form) or the adjacent chain amide group, correspondingly. These imine-ether units are sensitive to a Chapman recombination at the temperatures evaluated, which leads to the terminal lactam moiety,



Which, upon hydrolysis of the polymer, provides the di(v-carboxypentyl) amine. Decarboxylation, which seems to become the most interesting aspect of side-reaction since it provides vast amounts of carbon dioxide, was the outcome of contact between two carboxyl end groups: [5]



Levchik et al. stated that nylon 66, a polyamide formed by diacid and diamine, generates oligomeric segments and monomeric parts, usually linear or cyclic. As many researchers have noted, peptide bonds or alkyl amide bonds, which are aliphatic chains' comparably the weakest bond, are the bonds that primary chain scission occurs in the polymer. As important chain methods, cis elimination, intramolecular transfer, and homolytic scission have mostly been suggested. According to the researchers, no conclusive findings or kinetic calculations appear to confirm one of these degradation pathways over the others. Furthermore, it indicates that each mechanism's impact is dependent on the experimental conditions. [5]

2.7. Molecular Weight and Molecular Weight Distribution

Polyamides are combinations of polymer molecules of divergent molecular weights formed by polycondensation processes, as well as their dispersion typically includes a specified linear function as per the Schulz–Flory "most probable distribution" model [25]. One such distribution function could hypothetically be calculated out from the kinetics of the polymerization process, but statistical analyses seem to be more straightforward.

Extend of reaction, p , can be described as the reaction probability. This probability includes the initially existent reactive groups, which are $[NH_2]_0 + [COOH]_0$ and the fraction group, which can be represented as $2[NHCO] / ([NH_2]_0 + [COOH]_0)$. Therefore $1 - p$ value shows the portion of the unreacted groups. It is now essential to evaluate the probability that an arbitrarily chosen polymer molecule has exact λ linkages. The one linkage presence possibility is p . This probability holds for the other linkages which are present in the molecule. For any links existing in that molecule, the same probability holds. Therefore, the probability of λ linkages existing is p^λ . $1 - p$ is the probability value for the presence of unreacted groups in this molecule. Both probabilities' product value equals the entire molecules' presence probability. [26]

$$p_\lambda = p^\lambda(1 - p) \quad (17)$$

The ratio of all molecules with λ linkages is equivalent to this product. The equation determines the total number of molecules as shown:

$$S_\lambda = Sp^\lambda(1 - p) \quad (18)$$

Here, the total number of molecules is represented as S value. P_n can be written as N/S . The exact number of the monomeric groups transformed into the polymer is represented as N . Since S is equal to N/P_n and P_n is equal to:

$$P_n = \frac{1 + r + q}{(1 + r)(1 - p) + q} \quad (19)$$

or $r = 1$ and $q = 0$, S_λ can be written as:

$$S_\lambda = Np^\lambda(1 - p)^2 \quad (20)$$

This represents the linear step-growth polycondensation function for number distribution at p , the extent of reaction. In this circumstance, λ can be formulated as:

$$\lambda = n_\lambda - 1 \quad (21)$$

The groups that have linkage with λ linkages are shown as n_λ . $S_\lambda n_\lambda \bar{m}$ shows the weight of the polymer molecules composed of n_λ structural components, whereas \bar{m} represents the average mass value of the polymer's structural component. In order to find the total weight of the polymer molecule, the complete amount of structural component N , and the average mass value of the structural component's \bar{m} must be multiplied as $\bar{m}N$. Therefore, polymer molecules' weight ratio in terms of n_λ degree of polymerization can be written as: [5]

$$W_\lambda = S_\lambda n_\lambda / N \quad (22)$$

After combining these two equations, the molecular weight distribution equation is as follows:

$$W_\lambda = p^\lambda(1 - p)^2 = n_\lambda p_\lambda^{n_\lambda - 1} (1 - p)^2 \quad (23)$$

This equation developed by Flory [25] is the most probable and widely recognized molecular weight distribution formula. In order to define a polymer definitely in terms of molecular weight distribution, it is sufficient to introduce the relationship between the degree of polymerization n_λ with S_λ/S or W_λ . However, in many cases, a characterization of the average

degree of polymerization or molecular weight is acceptable and sufficient. Various averages may be different from one another. This difference is defined in the following equation as [5]

$$\bar{M}_x = \left[\frac{\sum y_i M_i^{\alpha+1}}{\sum y_i M_i} \right]^{1/\alpha} \quad (24)$$

Here, y_i is the molecule ratio, which has a molecular weight of M_i . In terms of molecular weight, there are three essential parameters for practical use such as Number average \bar{M}_n ($\alpha = -1$), Weight average \bar{M}_w ($\alpha = 1$) and Viscosity average \bar{M}_v ($0.5 < \alpha \leq 1$).

Osmometry or end-group titration method can be used to achieve the number average, light scattering method can be utilized for weight average, and viscometry can be used for viscosity average. [27]

Although it is a relative method, viscometry is the most practical and efficient method for analyzing the characteristics of polyamides. It is widely used, and intrinsic viscosity ($[\eta]$), can be determined by this method. Intrinsic viscosity is dependent on the molecular weight and shows the macromolecular coil's hydrodynamic volume. Definition of the intrinsic viscosity can be written as: [15]

$$\lim_{c \rightarrow 0} \eta_{red} = \lim_{c \rightarrow 0} \eta_{sp}/c = [\eta] \quad (25)$$

As a result, it is generally calculated by extrapolating the concentration dependence of decreased viscosity variables to zero polymer concentration. The most common Huggins [28] and Kraemer [29] equations are used for determining the $[\eta]$:

$$\eta_{sp}/c = [\eta] (1 + k_H[\eta]c) \quad (26)$$

$$\ln \eta_{sp}/c = [\eta] (1 - k_K[\eta]c) \quad (27)$$

Here, specific viscosity is represented with η_{sp} relative viscosity is represented with η_{rel} , c is the concentration value with the unit g/dl, and lastly, coefficients of Huggins and Kraemer are written as k_H and k_K and their sum is $k_H + k_K = 0.5$. For polyamides that have low molecular weight, this correlation may not hold. [30,31]

The intrinsic viscosity of a given polymer can be calculated by formulating the relationship between the intrinsic viscosity and average molecular weight: [15]

$$[\eta] = KM^a \quad (28)$$

Staudinger, Mark, Kuhn, Houwink, and Sakurada are some scientists whose names have been related to this equation. Those quantities a and K are polymer-solvent functions. The quantity a can hypothetically contain levels ranging from 0.5 to 2.0. A Gaussian molecular coil of unperturbed dimensions could approximate the reduced number (impermeable, no excluded volume, u -conditions). A rodlike structure is represented by such a value of 2. Aliphatic polyamides are a type of extensible macromolecule with a quantity ranging from 0.5 to 0.9. More significant results were expressed since the molecular coil increases in strong solvents. Table 1 [18,32-42] represents many of the published results for the quantities K and a (equation 28). A much more comprehensive list has also been released, and therefore a clear explanation of molecular weight computation and concentrated solution properties of aliphatic polyamides. [5]

Parameters for Mark-Houwink Equation: $[\eta] = KM^a$

Solvent	Temperature (°C)	Calibration method	MW range ($M \times 10^{-3}$)	$10^4 K$ dl/g	a	Ref.
<i>Nylon-4</i>						
<i>m</i> -Cresol	25	LS (M_w)	10–300	4.0	0.77	32
<i>m</i> -Cresol	25	EG (M_n)	1.7–14	30.0	0.70	33
<i>Nylon-6</i>						
<i>m</i> -Cresol	25	LS (M_w)	5–40	5.57	0.73	34
<i>m</i> -Cresol	25	LS (M_w)	9–335	5.26	0.74	35
<i>m</i> -Cresol	25	EG (M_n)	5–30	18.0	0.65	34
Tricresol	25	OS (M_w)	8–80	2.1	0.90	36
Conc. H ₂ SO ₄	25	EG (M_w)	4–37	6.3	0.76	37
85% HCOOH	20	V (M_v)	7–120	2.26	0.82	38
CF ₃ CH ₂ OH	25	V (M_v)	13–100	5.36	0.75	38
<i>Nylon-6,6</i>						
<i>m</i> -Cresol	25	LS (M_w)	7–80	24.0	0.61	39
90% HCOOH + 2M KCl	25	LS (M_w)	2.5–50	14.2	0.56	40
90% HCOOH	25	EG (M_n)	6–24	11.0	0.72	41
<i>m</i> -Cresol	20	V (M_v)	10–40	38.0	0.55	42
<i>Nylon-6,10</i>						
<i>m</i> -Cresol	25	EG (M_w)	8–24	1.35	0.96	43
<i>Nylon-8</i>						
<i>m</i> -Cresol	25	EG (M_w)	1–25	7.0	0.76	44
<i>Nylon-12</i>						
<i>m</i> -Cresol	25	LS (M_w)	3–125	8.1	0.70	45
<i>m</i> -Cresol	25	EG (M_n)	1–33	11.8	0.73	45

Table 1 . Parameters for Mark-Houwink Equation

The average molecular weights that were defined earlier are in correlation with the average degrees of polymerization value p_λ . These average molecular weight values are generally applied in the calculations of the extent of reaction p . Number average value \bar{P}_n and the average weight value P_w are the most critical average values. These average values can be

formulated as [5,26,27]

$$\bar{P}_n = \left(\sum_{\lambda} S_{\lambda} n_{\lambda} \right) / \left(\sum_{\lambda} S_{\lambda} \right) = \sum p_{\lambda} n_{\lambda} \quad (29)$$

$$P_w = \left(\sum_{\lambda} S_{\lambda} n_{\lambda}^2 \right) / \left(\sum_{\lambda} S_{\lambda} n_{\lambda} \right) = \sum w_{\lambda} n_{\lambda} \quad (30)$$

Implementing the eq. 28 and eq. 23 into those equations respectively, and calculating the summation equations, the formulas become:

$$\sum_{\lambda} n_{\lambda} p_{\lambda}^{n-1} (1-p), \quad (31)$$

$$\sum_{\lambda} n_{\lambda}^2 p_{\lambda}^{n-1} (1-p)^2 \quad (32)$$

Applying the $p < 1$ boundary condition, the equations can be written as:

$$\bar{P}_n = \frac{1}{1-p} \quad (33)$$

$$\bar{P}_w = \frac{1+p}{1-p} \quad (34)$$

According to the above equations, $\bar{P}_w/\bar{P}_n = 1 + p$, which is equal to \bar{M}_w/\bar{M}_n and both of these equations indicate the polydispersity index. When this polydispersity index is applied to linear polyamides, it approaches 2 as the extent of the reaction is expanded. Minor variations which are considered negligible have occurred in the \bar{P}_w/\bar{P}_n ratio due to the modification of \bar{P}_w and \bar{P}_n values depending on the nonstoichiometric concentration of bifunctional reactants as well as the inclusion of monofunctional species. In order to control and actualize the polymerization process, the process of fiber formation, due to important effects on rheological polymer properties of polyamide melts and the characteristics of the finished product, especially in relation to the tensile properties of the finished product, molecular weight, final viscosity, and molecular weight distribution play critical roles. Thus, it is necessary to determine more than one molecular weight to characterize and inspect the polymer appropriately. [5,43]

CHAPTER 3

FORMULATION OF CFD MODEL

3.1. Governing Equations

In this thesis, Kordsa facilities' polyamide 66 line was studied; therefore, single-phase high viscosity reacting flow model is used for the computations.

Since this flow includes reaction, a heat transfer model is added to simulate the reaction and the viscosity build-up depending on the reaction profile. To obtain accurate results, experimental data is used for reaction modeling, and a curve fit function is used for temperature – viscosity relationship. For the single-phase high shear laminar flow, the below equations are used:

3.2. Conservation of Mass

The continuity equation for laminar flow is as follows:

$$\nabla \cdot (\rho u) = 0 \quad (35)$$

Where u is the velocity vector in (m/s) and ρ in (kg/m^3) is the density of the fluid.

3.3. Conservation of Momentum

The momentum balance equation for laminar flow is as follows:

$$\rho(u \cdot \nabla)u = \nabla \cdot [-pI + K] + F \quad (36)$$

Here, p is pressure in (Pa) , I is the identity matrix, K is the viscous stress tensor in (Pa) , and F is the volume force vector in (N/m^3) .

3.4. Heat Transfer

Following heat transfer equations are solved for heat transfer calculations:

$$\rho C_p \left(\frac{\partial T}{\partial t} + u \cdot \nabla T \right) + \nabla \cdot (q + q_r) = \alpha_p T \left(\frac{\partial p}{\partial t} + u \cdot \nabla p \right) + \tau : \nabla u + Q \quad (37)$$

$$\alpha_p = -\frac{1}{\rho} \frac{\partial \rho}{\partial t} \quad (38)$$

$$Q_p = \alpha_p T \left(\frac{\partial p}{\partial t} + u \cdot \nabla p \right) \quad (39)$$

$$Q_{vd} = \tau : \nabla \mathbf{u} \quad (40)$$

3.5. Chemical Reaction Model

Two different methods can be used to create the chemical reaction model. The first of these is to solve the formulas covering all polyamide 66 reaction dynamics defined in Chapter 2 by solving them by the help of COMSOL program. The second option is to take samples from the sample and purge collection points located at certain intervals in the existing polymerization line, measure the viscosity values in the Kordsa laboratory, and create a curve fit equation by matching the temperature values on the line. The second method was used for modeling the chemical reaction in order to model the Kordsa polymerization line in one-to-one similarity and to ensure that the polymerization characteristics in the line are as accurate and precise as possible. Therefore, no information was given about the molarities of the released products. The rate of the chemical reaction can only be followed from the viscosity increase rate. The exact temperature and viscosity values are not given due to confidentiality reasons.

As shown in the graph, the value of viscosity rises as the temperature of the polymer increases. As previously stated in the rheology section, the polyamide reaction progresses as the temperature rises and water is removed from the environment and the molecular weight increases as a result of this progression. The increase in molecular weight has the same effect on viscosity as in formulae.

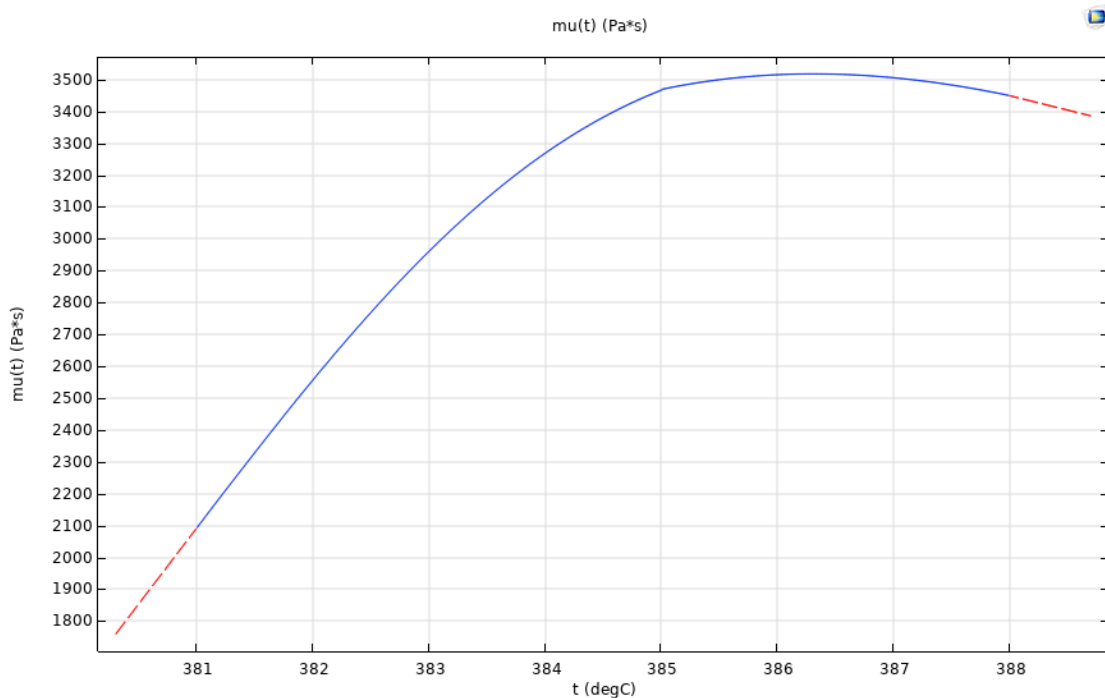


Figure 1 . Chemical Reaction Curve Fit Graph

As seen in the graph, the viscosity value gradually returns after a specific temperature value. Because of thermal degradation, the molecular weight and viscosity of the polyamide 66 polymers can no longer be increased beyond a certain point.

3.6. CFD Model

In this thesis, the final zone of the Kordsa Polyamide 66 Continuous Polymerization Line is studied. This continuous polymerization line's final section has spare equipment for all of its polymerization equipment, which allows maintenance work to continue at regular intervals by swapping out the equipment at different times. The fact that these equipment replacement operations are carried out during the manufacture of molten polymer without interrupting the process means that there are three-way valves installed on the line that routes the polymer from one piece of equipment to the other piece of equipment. There are nozzles within these three-way valves, allowing the polymer to flow more rapidly. While doing CFD analyses, nozzles with varying constriction shapes were investigated and compared to the polymer flow in a straight pipeline to see which was more efficient. The viscosity build-up profile is the most important metric to consider when comparing flow rates: It is possible to simulate how this profile varies depending on the nozzle type.

3.7. Geometry

Four distinct nozzle types were tested to determine the influence of polymer flow, heat transfer, and viscosity increase on the effects of nozzle type and line contractions on polymer flow, heat transfer, and viscosity rise. One of these nozzle types is designed as a straight line to observe how the flow and viscosity profile of the polymer is formed in the absence of any line contraction or nozzle.

3.8. Current Nozzle Design

The current nozzle design is identical to the nozzle design used in the polymerization line, with the dimensions slightly different because of the need to maintain confidentiality. The inlet diameter of the nozzle used in the study is 100 mm and is reduced to a diameter of 60 mm by narrowing at an angle of 5 degrees. Polymer continues to flow along a diameter of 60 millimeters for 500 millimeters, turns 90-degree after an elbow bent, and continues for another 500 millimeters. Upon reaching the end of 500 mm, the polymerization line expands at an angle of 5 degrees and returns to its original size of 100 mm in the exit diameter.

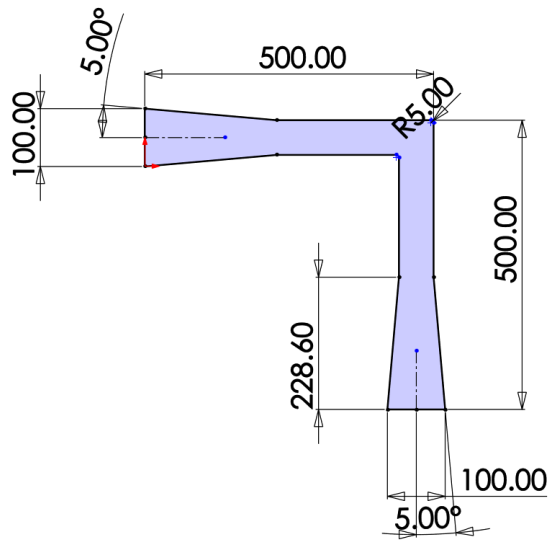


Figure 2 . Current Design Geometry

3.9. Narrow-Angle Nozzle Design

The second nozzle design is similar to the first design, with the exception that the diameter narrowing in the pipeline is achieved by the use of a greater angle. For the second design, the influence of the early and rapid contraction in the pipeline, which narrowed by 15 degrees, on the polymer flow, temperature, and viscosity is evaluated. The inlet diameter of the nozzle used in the study is 100 mm and is reduced to a diameter of 60 mm by narrowing at an angle of 15 degrees. Polymer continues to flow along a diameter of 60 millimeters for 500 millimeters, turns 90-degree after an elbow bent, and continues for another 500 millimeters. Upon reaching the end of 500 mm, the polymerization line expands at an angle of 15 degrees and returns to its original size of 100 mm in the exit diameter.

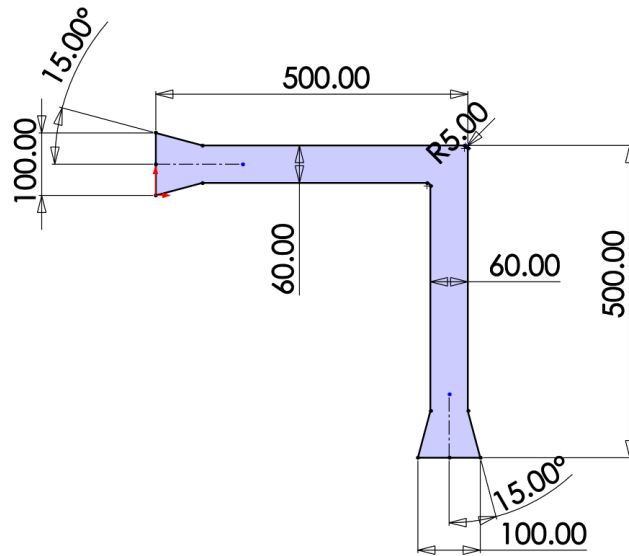


Figure 3 . Narrow-Angle Design Geometry

3.10. Wide Angle Nozzle Design

The purpose of the third nozzle design, designed with a wide-angle, is to gradually create an uninterrupted contraction up to the elbow section without creating a sudden contraction. The inlet diameter is 100 mm as in the other lines, and the diameter narrowing continues gradually with an angle of approximately 2.3 degrees along the 500 mm line, turns 90-degree after an elbow bent, gradually increases the angle by about 2.3 degrees after the elbow section and reaches 100 mm again at the exit point. The flow, temperature, and viscosity profiles of the polymer, which are not subject to sudden and short-term contraction, were investigated in this design.

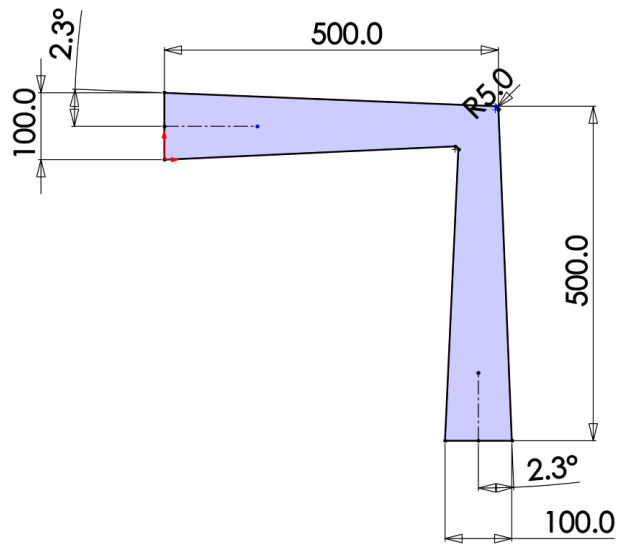


Figure 4 . Wide Angle Design Geometry

3.11. Straight Line Design

The final pipeline design, in which no line constriction is added, is designed to observe the polymer's velocity, temperature, and viscosity distribution without the constriction effects. With an inlet diameter of 100 mm, this pipeline continues straight for 500 mm without any contraction, turns 90-degree after an elbow bent, continues as a straight line of 500 mm, and exits with a diameter of 100 mm.

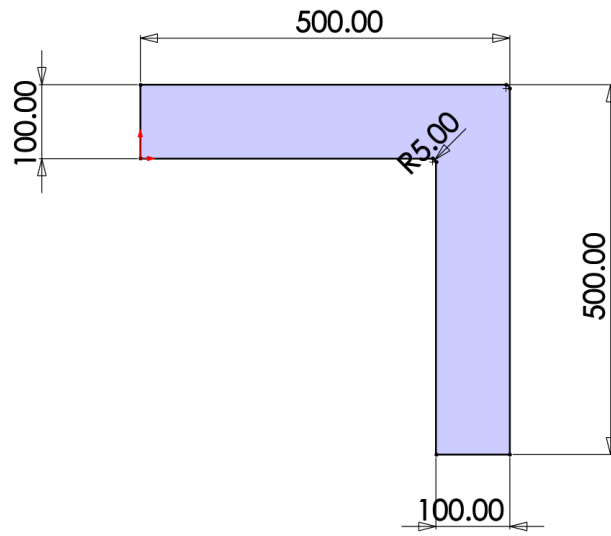


Figure 5 . Straight Line Geometry

	Current Design	Wide Angle	Narrow Angle	Straight Line
Inlet	100 mm	100 mm	100 mm	100 mm
Outlet	100 mm	100 mm	100 mm	100 mm
Contraction Diameter	60 mm	60 mm	60 mm	-
Contraction Angle	5°	2.3°	15°	-

Table 2 . Design Parameters of the Nozzles

3.12. Boundary Conditions

3.13. Wall

No-slip boundary condition $u = 0$ is preferred due to the viscous flow of the fluid.

3.14. Inlet

The normal inflow boundary condition is used in the inlet of the nozzles. The fluid inlet velocity was chosen to be 0.1 m/s, similar to what it was in the polymer production line.

3.15. Outlet

A zero-pressure boundary condition is used in the outlet of the pipe.

$$[-pI + K]n = -\hat{p}_0 n \quad (41)$$

$$\hat{p}_0 \leq p_0 \quad (42)$$

3.16. Wall Temperature Boundary Condition

As with the polymerization line, the simulation defines the boundary conditions for heating from the pipe walls. For confidentiality considerations, the temperature of the pipeline walls was chosen to be different from that of the current polymer lines. The pipe wall temperature is set to 655 K in the current scenario. $T = T_0$

3.17. Inflow Heat Boundary Condition

The temperature of the polymer at the point of entry into the pipeline was set at 652 K. To maintain confidentiality, the same temperature values as those used in the polymerization line are not included in the computations. The following are the formulas used in the computation of inflow boundary conditions.

$$-n \cdot q = d_z \rho \Delta H u \cdot n \quad (43)$$

$$\Delta H = \int_{T_{ustr}}^T C_p dT \quad (44)$$

3.18. Outflow Heat Boundary Condition

The output boundary condition was chosen for the heat dissipation profile formed towards the flow direction of the polymer after heat transfer as follows.

3.20. Mesh

Mesh properties are selected as follows:

Description	Value
Minimum element quality	0.3358
Average element quality	0.7983
Triangle	1503
Quad	334
Edge element	189
Vertex element	18

Table 3 . Mesh Properties

Description	Value
Calibrate for	Fluid dynamics
Maximum element size	25.3
Minimum element size	1.13
Curvature factor	0.4
Maximum element growth rate	1.2
Predefined size	Coarse

Table 4 . Mesh Size

CHAPTER 4

CFD PROGRAM VALIDATION ANALYSIS

4.1. CFD Validation Calculations

The study conducted by Ease and Barigou [44] was used as an example to verify the accuracy and reliability of the analyses and calculations performed using the COMSOL program. The findings obtained through the COMSOL software, and the results obtained through equations 45 and 46 were compared.

The following precise equation describes the volumetric flow rate (Q) of a power-law fluid in a pipe [45]

$$Q = \frac{n\pi R^3}{(3n + 1)} \left(\frac{R}{2k} \cdot \frac{\Delta P}{L} \right)^{1/n} \quad (45)$$

Here, R is the radius of the pipe, and $\frac{\Delta P}{L}$ is the pressure drop per unit length. The fluid velocity profile can be derived as follows, where r is the radial position.

$$u(r) = \frac{n}{n + 1} \left(\frac{\Delta P \cdot R}{2kL} \right)^{1/n} R \left[1 - \left(\frac{r}{R} \right)^{\frac{n+1}{n}} \right] \quad (46)$$

In equation (45), all the variables except pressure drop per unit length are known. Therefore, using the equation (45), pressure drop per unit length is calculated. The calculated pressure drop per unit length value is inserted into equation (46), and then a fully developed fluid velocity profile calculation is made for different r values. The same analytical calculations were made in the CFD program, and these results were compared.

Analytical and CFD calculations were performed for two different cases. Power-law fluids with different fluid consistency coefficients and flow behavior index values were selected in the calculations and analyzes were performed according to different input speeds. As seen in Figure (12), analytical and CFD calculations are the same. The fact that these values are the same shows that the CFD program is sufficient for modeling the given single-phase non-Newtonian flow. The basis for these calculations is Ease and Barigou [44].

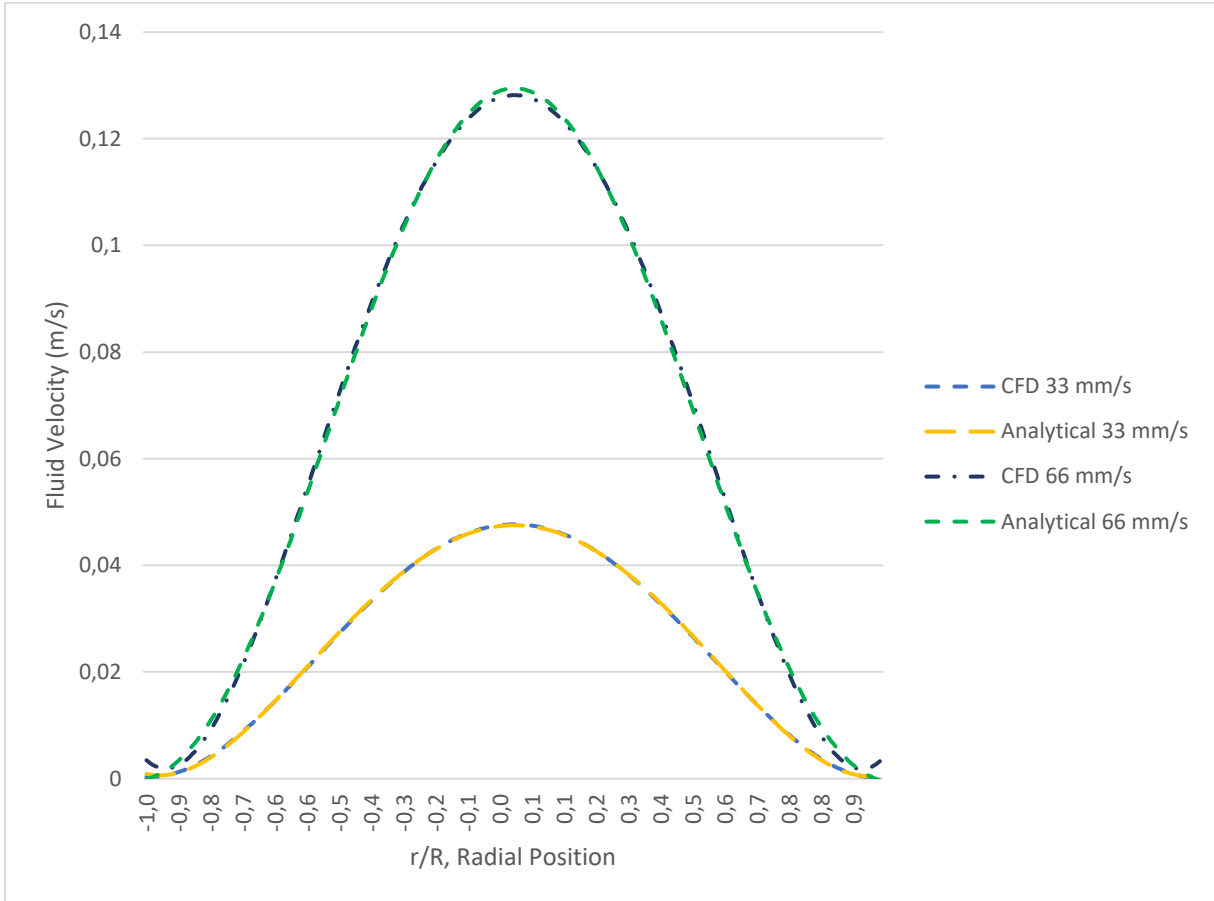


Figure 6 . Comparison of theoretically calculated and CFD velocity profiles for a power-law fluid flowing alone: for $V_{in} = 66 \text{ mms}^{-1}$ ($k = 0.16 \text{ Pa} * \text{s}^n, n = 0.81$) and $V_{in} = 33 \text{ mms}^{-1}$ ($k = 0.75 \text{ Pa} * \text{s}^n, n = 0.71$)

4.2 Mesh Dependency Analysis

In order to show that the CFD analysis is independent from the mesh, analyzes were made with different mesh numbers and the results were compared. Initially, the mesh number was chosen as 5257, then refined as 13884 and 15461 and applied to the entire geometry. Since the simulation results did not change after these refinements, the economically suitable mesh number of 5257 was preferred. This selected mesh number was applied for four different nozzle types.

CHAPTER 5

RESULTS AND DISCUSSION

The focus of the computational study in this thesis is heat transfer and the change in the viscosity profile within the poly-condensation process. The relevant governing equations describing the physics in this problem are solved by using the Comsol program after defining geometrical parameters of the computational domain, boundary conditions and transport properties. Computational study is realized for four different nozzle geometry designs. In all four configurations investigated, the inlet, outflow, wall boundary conditions, and material parameters are kept constant. The effect of nozzle geometry on flow and heat transfer profile is investigated in detail. It is observed that depending on the nozzle geometry, different heat transfer behaviors occur in the polycondensation process, and this causes the polymer to have disparate viscosity increase profiles. The variation of the viscosity profile depending on the nozzle geometry is due to the reduction in the diameter of the inlet and outlet section of the nozzle geometry, which increases heat transfer in the flow domain. With the increased heat transfer, the poly-condensation chemical reaction accelerates, thus causing an increase in viscosity and the development of different viscosity profiles. As elaborated in Section 2, exposing the polymer to high temperature suddenly might result in cross-linking and gel formation. The sudden temperature rise might affect the viscosity build-up profile, resulting in a range of viscosity increase profiles over the polymerization line.

5.1 Case 1 – Current Nozzle Design

As stated in the Section 3, where boundary conditions are defined, the polymeric fluid enters the nozzle with a velocity of 0.1 m/s reaches a fully developed flow profile where the maximum velocity is 0.16 m/s at the center point. Since the wall boundary conditions are defined as no-slip, the relative velocity at the walls is calculated as 0 m/s as seen in the velocity contour plot. Flow profile graphs obtained according to the inlet and outlet boundary conditions are as follows.

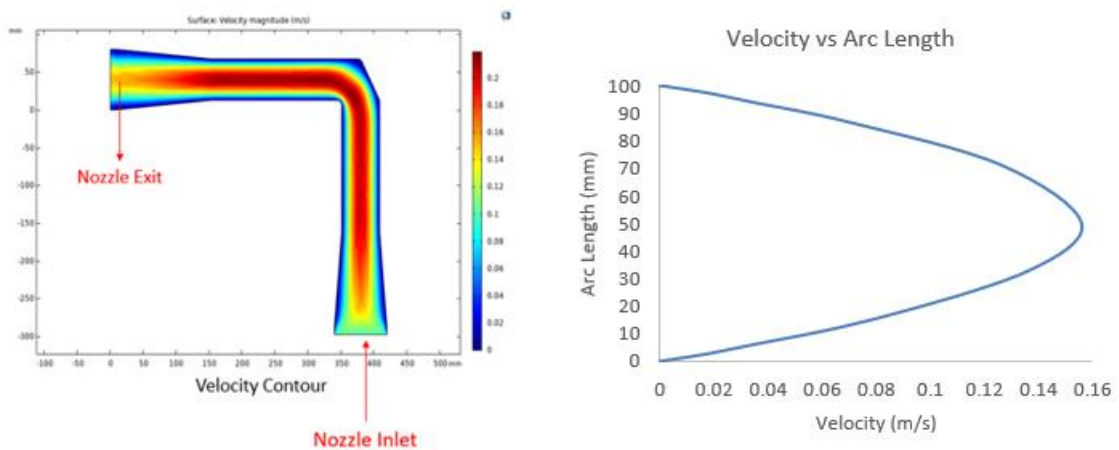


Figure 7 . Current Design Velocity Profile Contour and Profile

As with all four nozzle designs, the wall temperature boundary condition was chosen as 655 K. The polymeric fluid enters the nozzle at a temperature of 652 K. As can be seen in the temperature contour and temperature profile graphs below, the nozzle walls have the highest temperature values due to both zero relative flow and being the closest region to the heat transfer source. The center of the polymeric liquid has lower temperature values than the walls because it is far from the heat source. The temperature increases along the line in the flow direction.

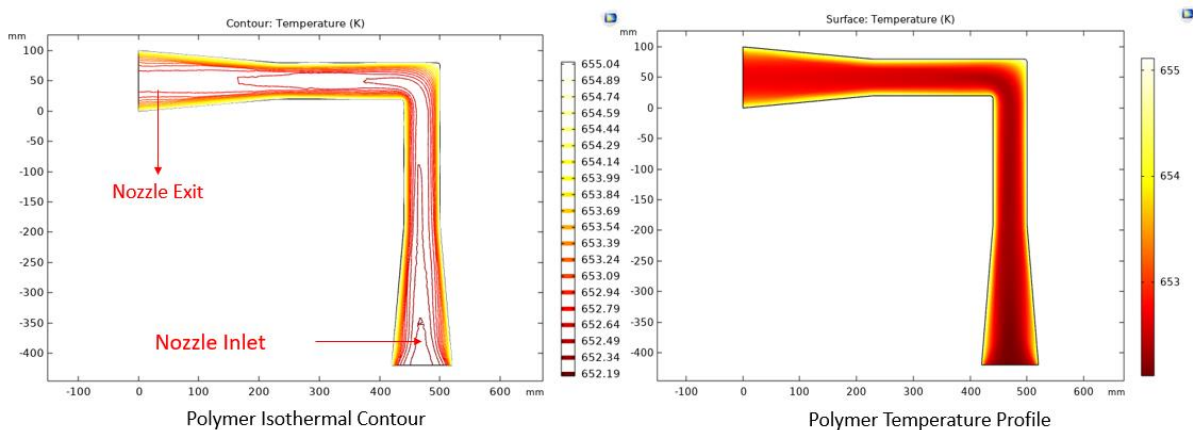


Figure 8 . Current Design Isothermal Contour Graph and Temperature Profile Graph

Due to the furtherance of heat transfer and temperature increase along the pipeline, the chemical reaction also continues, and as a result, the viscosity of the polymer increases. As can be seen in the graphic below, the polymer viscosity increases along the outlet nozzle line. The red dots are the points from which each viscosity data is sampled. The viscosity value at the first measurement point of the outlet line is $1633 \text{ Pa} \cdot \text{s}$, and the viscosity value after the build-up with the reaction at the end of the outlet line is $1738 \text{ Pa} \cdot \text{s}$.

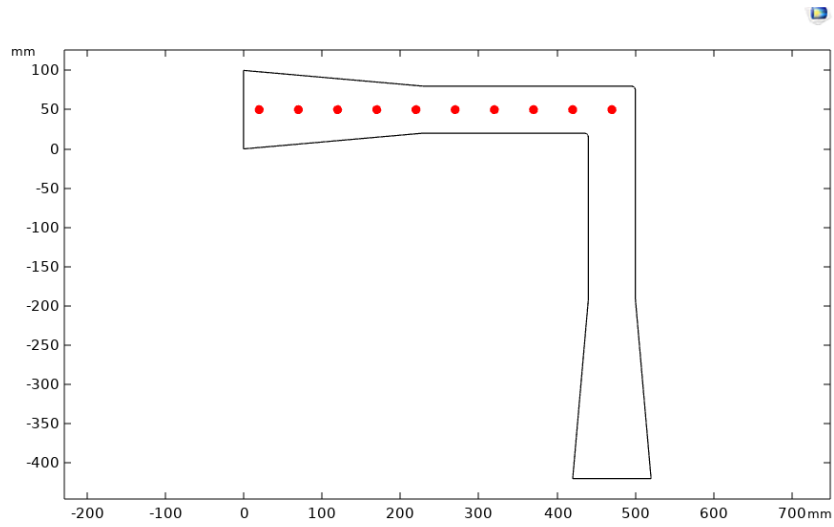


Figure 9 . Current Design Viscosity Data Points

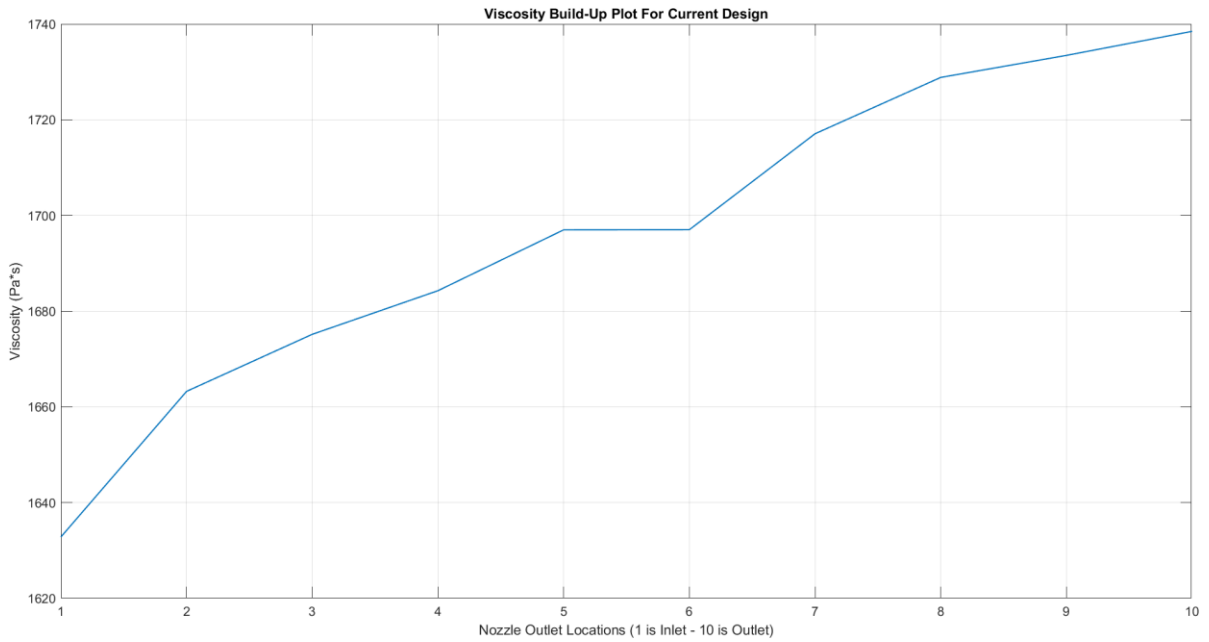


Figure 10 . Current Design Viscosity Build Up Profile

5.2 Case 2 – Narrow-Angle Nozzle Design

As stated in the section where boundary conditions are defined, the polymeric fluid enters the nozzle with a velocity of 0.1 m/s reaches a fully developed flow profile and achieves a maximum velocity of 0.17 m/s at the center point. Since the wall boundary conditions are defined as no-slip, the relative velocity at the walls is calculated as 0 m/s as seen in the velocity contour plot. Flow profile graphs obtained according to the inlet and outlet boundary conditions are as follows.

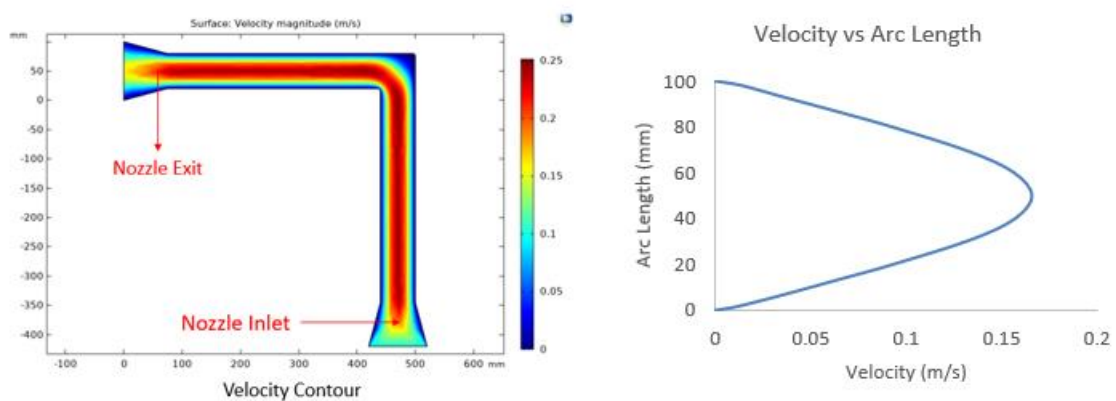


Figure 11 . Narrow-Angle Design Velocity Profile Contour and Profile

As in the first design, a temperature of 655 K is observed at the line walls, while towards the center of the line, this temperature is at the level of 652 K. Since the line is narrower, the effect of heat transfer is higher compared to the wider nozzle designs. Therefore, the reaction dynamics and viscosity build-up are different from the current design.

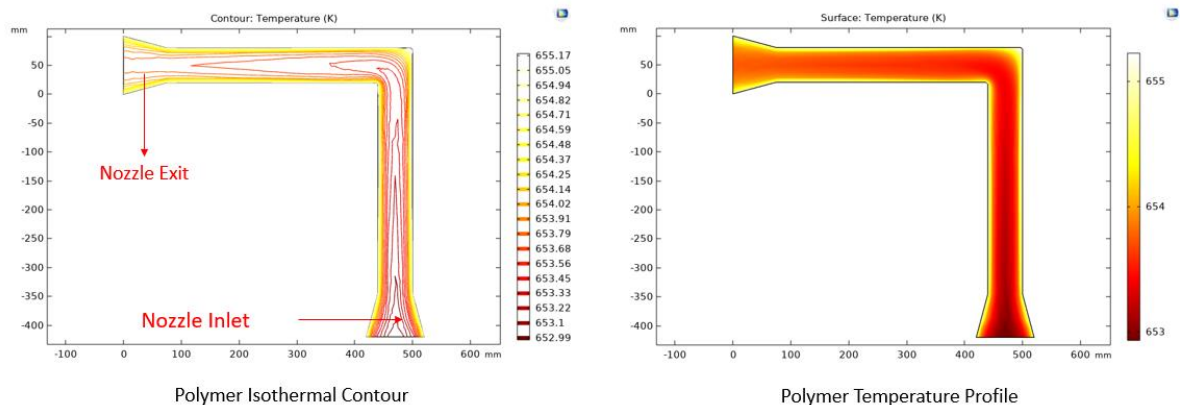


Figure 12 . Narrow-Angle Design Isothermal Contour Graph and Temperature Profile Graph

As a result of the chemical reaction that carries on with the continuation of heat transfer, the viscosity of the polymer increases, as can be seen in the figure (19) below. The polymer viscosity values were taken from 10 different points on Comsol CFD software, and the viscosity increase curve was calculated by evaluating these values on the graph. The polymer viscosity value observed at the first point of the outlet line is 1774 Pa*s, and the viscosity value observed at the end of the outlet line is 1896 Pa*s.

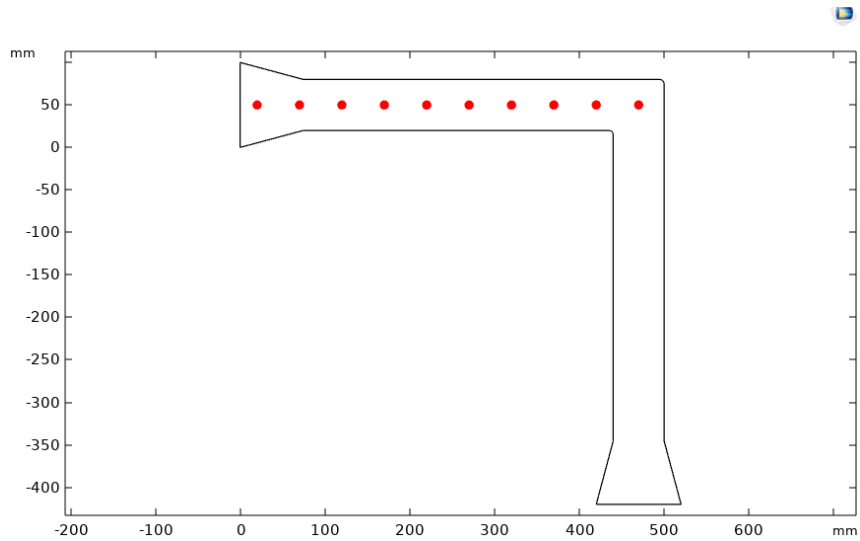


Figure 13 . Narrow-Angle Design Viscosity Data Points

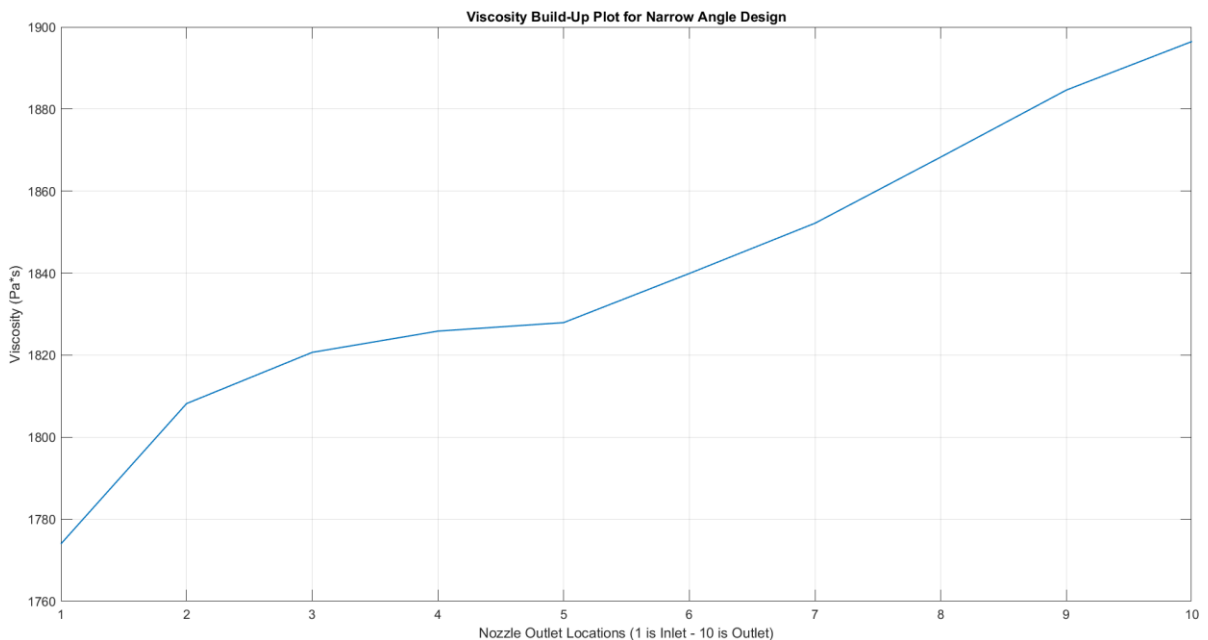


Figure 14 . Narrow-Angle Design Viscosity Build Up Profile

5.3 Case 3 – Wide-Angle Nozzle Design

As in the graphs below, the polymer enters the line at a speed of 0.1 m/s, as in other nozzle designs, and achieves a speed of 0.15 m/s in the center after obtaining a fully developed flow profile. Since the wall boundary conditions are no-slip, the relative velocity of the fluid in the wall is 0 m/s.

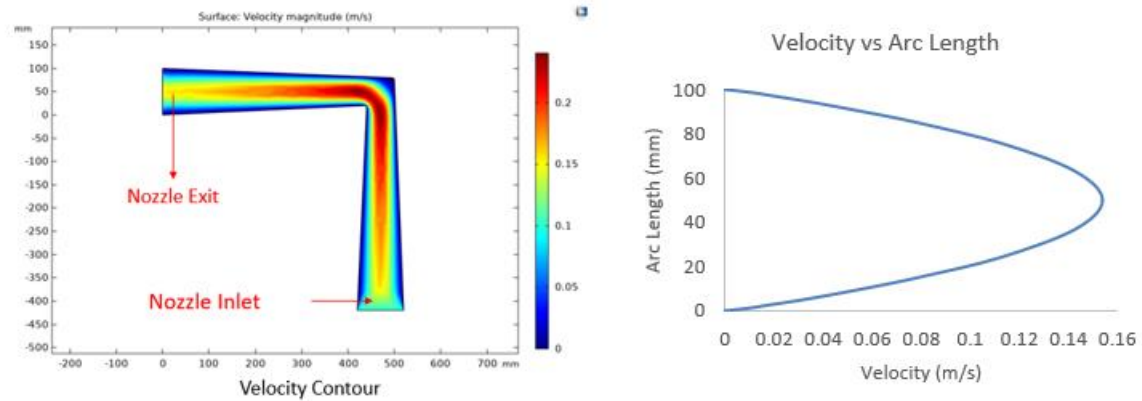


Figure 15 . Wide Angle Design Velocity Profile Contour and Profile

The temperature variation of the polymeric liquid across the nozzle is different from the first two designs, as no sudden diameter shrinkage is observed. Although the reaction continues because heat transfer continues, the viscosity increase also differs from other nozzles due to the different temperature distribution.

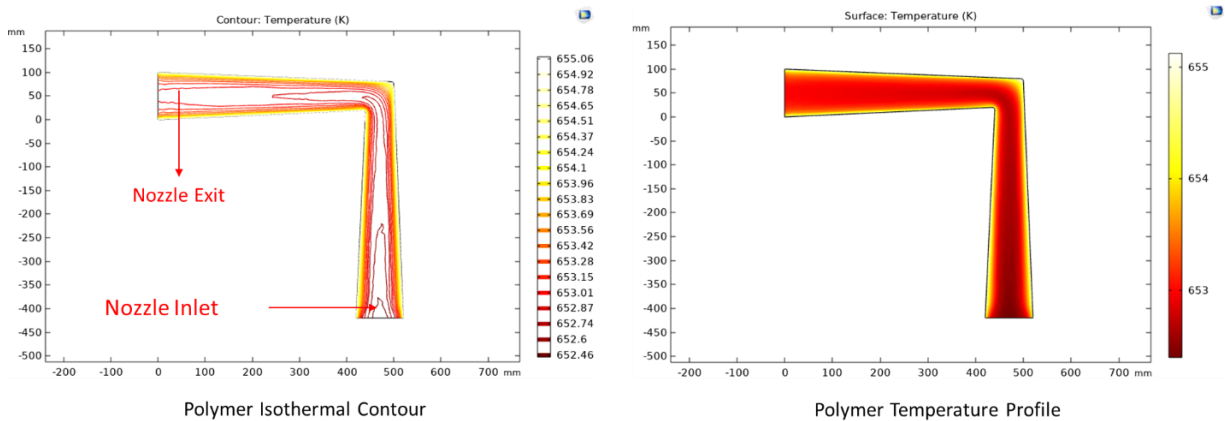


Figure 16 . Wide Angle Design Isothermal Contour Graph and Temperature Profile Graph

The viscosity of the polymer rises as a result of the chemical reaction that continues to occur in conjunction with the continuation of heat transfer. Figure (23) shows that polymer viscosity measurements were obtained from ten different points on the Comsol CFD program, and that the viscosity rise curve was derived by evaluating these data on the graph. The viscosity of the polymer was measured at the first point of the outlet line and the end of the outlet line.

The first point of the outlet line measured 1532 Pa*s, and the last point measured 1606 Pa*s.

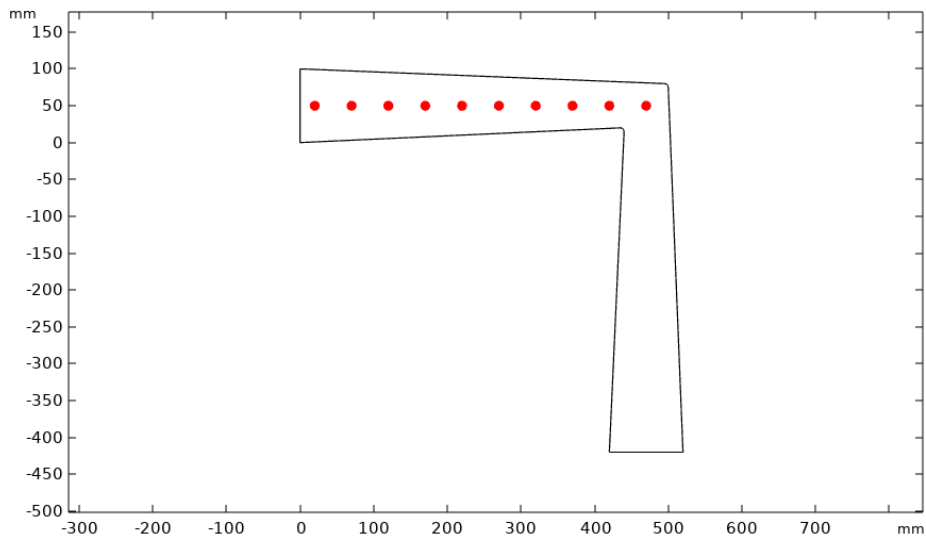


Figure 17 . Wide Angle Design Viscosity Data Points

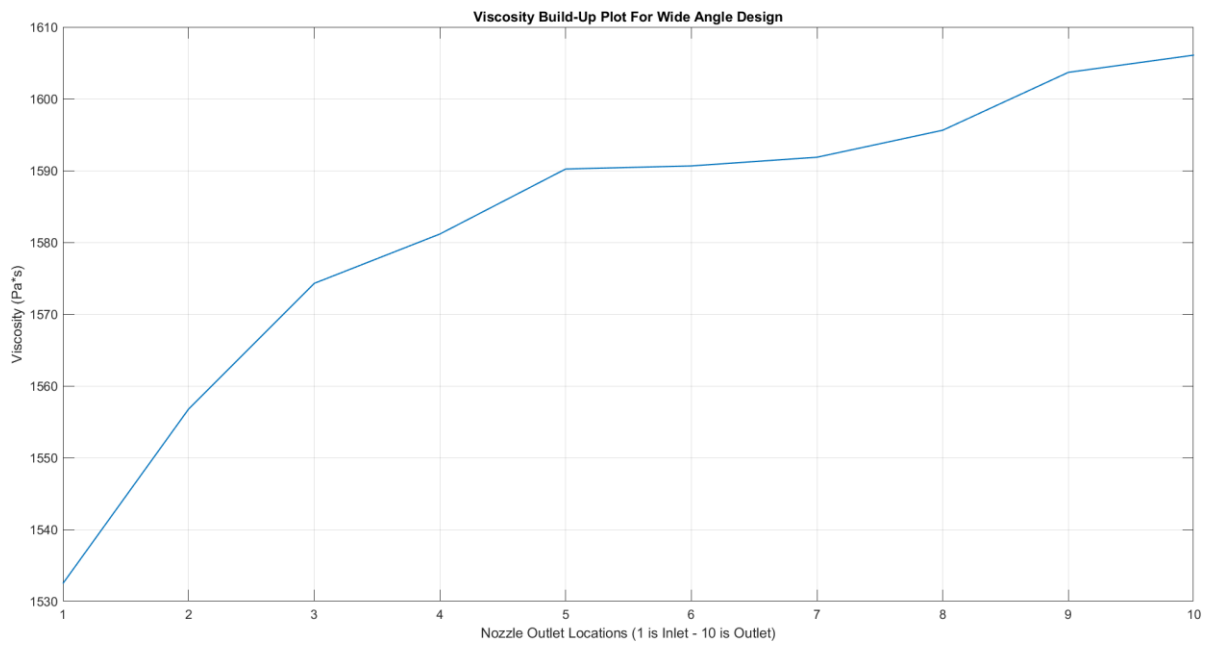


Figure 18 . Wide Angle Design Viscosity Build Up Profile

5.4 Case 4 – Straight Line Design

The polymer enters the pipeline with a velocity of 0.1 m/s and reaches a velocity of 0.16 m/s in the center after obtaining the fully developed profile. Since there is a no-slip boundary condition on the pipe walls, the relative polymer velocity on the walls is 0 m/s.

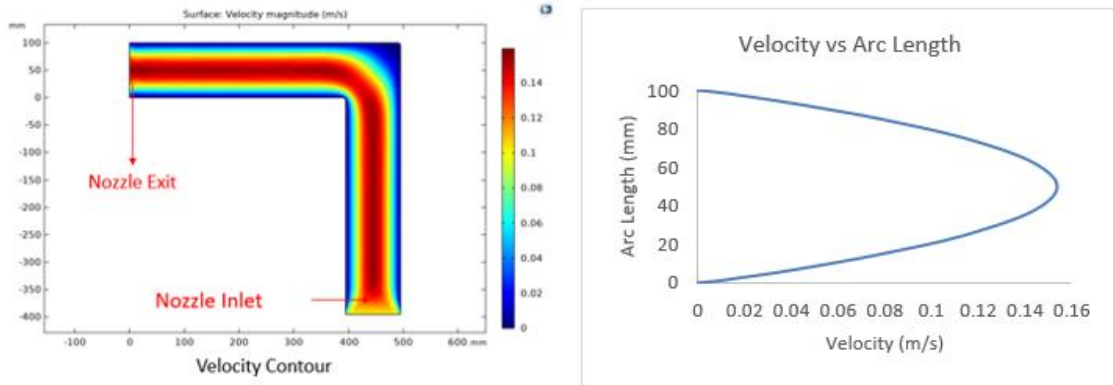


Figure 19 . Wide Angle Design Velocity Profile Contour and Profile

The temperature at the pipe walls is 655 K, which is the same as it was in all initial designs. The temperature of the pipe reaches 652 K as it approaches the middle of the pipe. There is no nozzle design in the pipeline, which means the impact of heat transfer is lesser than it would be with other designs. As a result, the output temperature remains at a lower level compared to other designs.

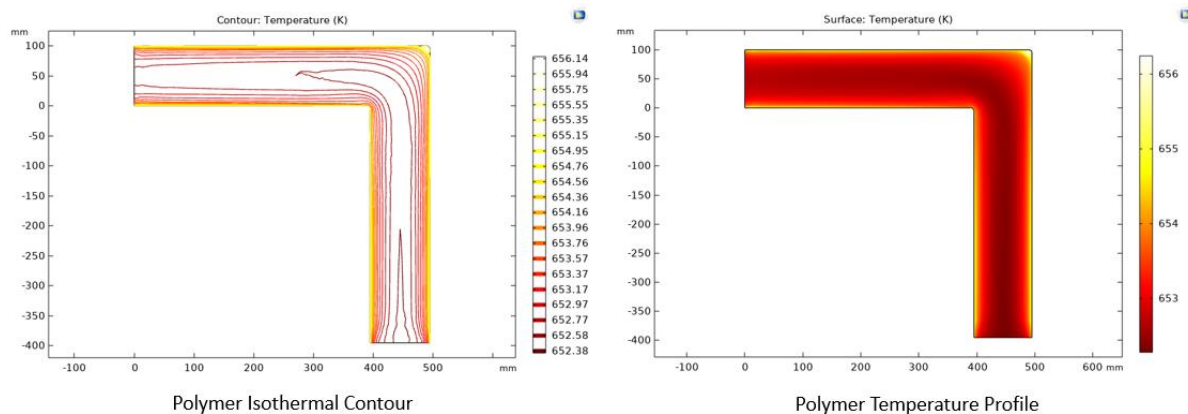


Figure 20 . Straight Line Design Isothermal Contour Graph and Temperature Profile Graph

The chemical reaction proceeds as a result of the continuing heat transfer, and as a result, an increase in viscosity is observed. The viscosity build-up graph, which is created by combining data from 10 separate locations, depicts the reaction properties of the polymer under consideration. The entrance viscosity of the pipeline was measured at 1390 Pa*s, while the output viscosity was measured at 1492 Pa*s.

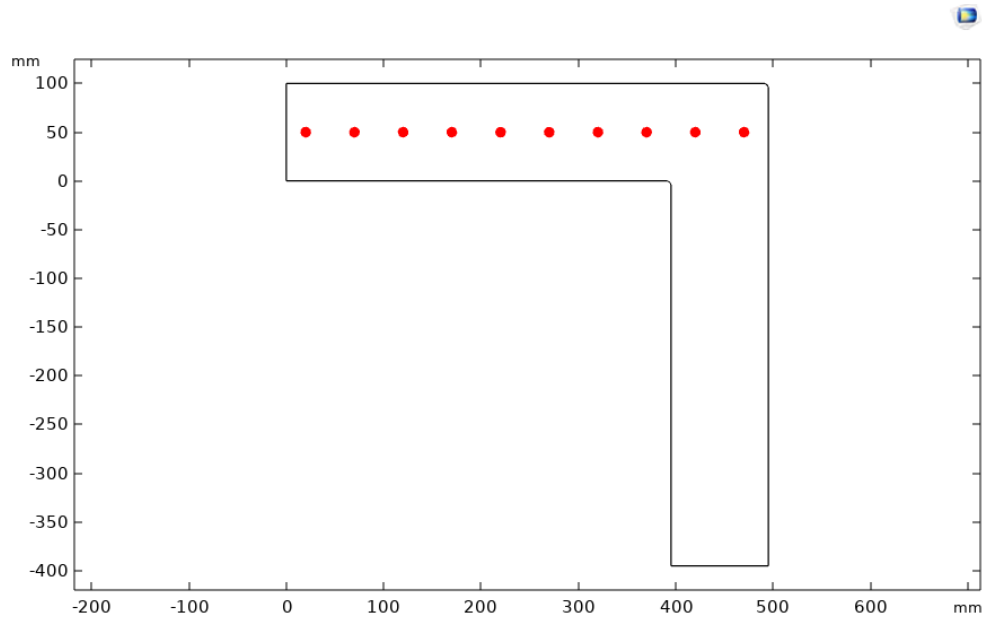


Figure 21 . Straight Line Design Viscosity Data Points

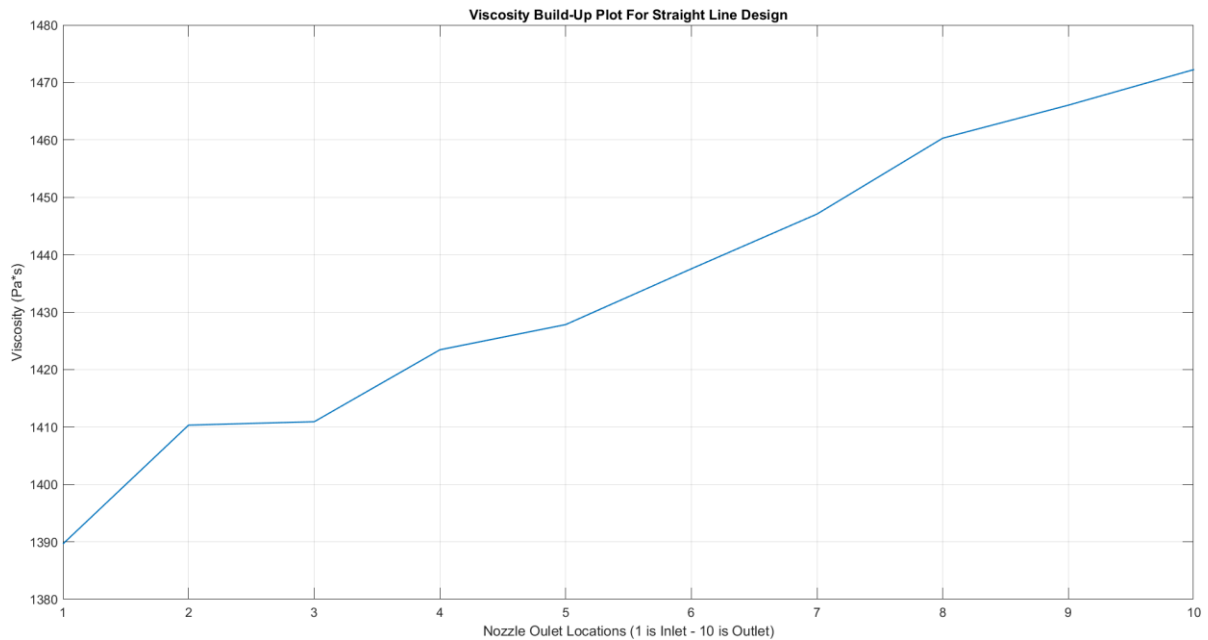


Figure 22 . Straight Line Design Viscosity Build Up Profile

5.5 Comparison

The fully developed velocity profile obtained from the flow modeling of four distinctive designs is as follows. Because the pipes' inlet and outlet geometries and their inlet velocity boundary conditions are the same in all four configurations, the outlet velocity profiles are similar in all four designs. However, the output velocity of the narrow angle nozzle design, which has a diameter narrowing with a high angle and travels long distances with narrowed line diameter, is higher than other nozzle designs due to geometry. No significant difference was observed in the output velocity in straight line, current design, and low angle nozzle designs.

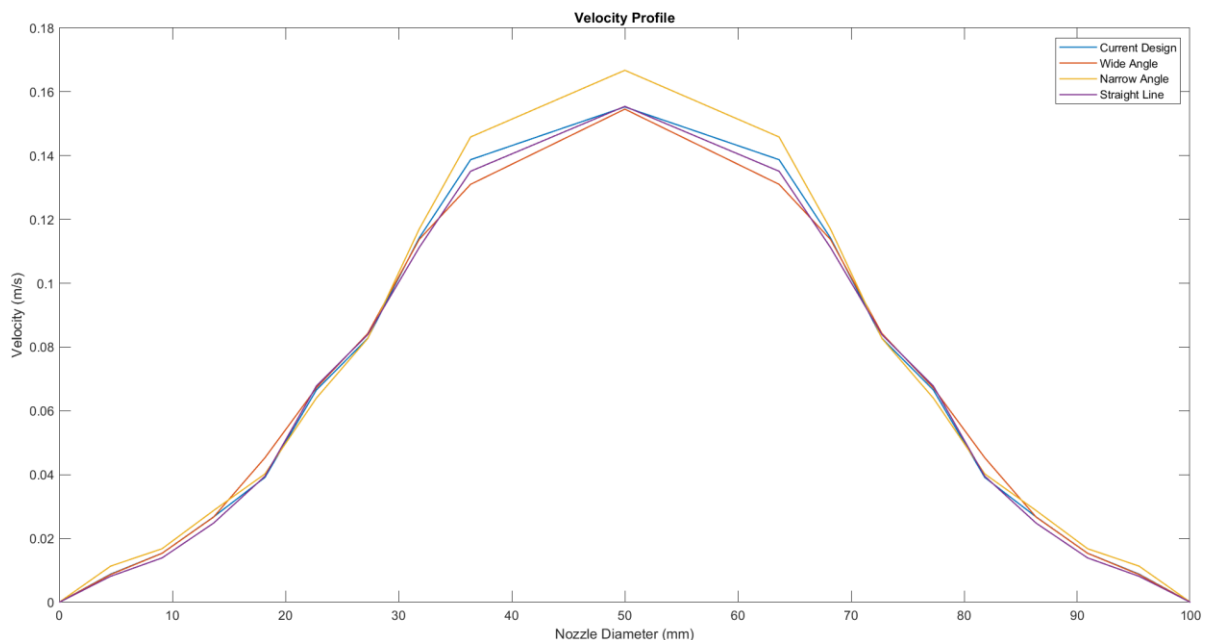


Figure 23 . Nozzle Outlet Velocity Profile Comparison

In order to examine the effect of the nozzle geometry on the polymer exit temperature, a temperature profile was obtained from the nozzle outlet region, as seen in figure (30). Accordingly, although the temperature value at the pipe wall is the same in all designs, the temperature in the pipe center is observed at the lowest in the straight pipeline since its center is the furthest to the pipe walls, while the highest temperature is observed in the narrow-angle nozzle design in which the polymer comes closest to the pipe walls, which are the heat source. The difference in this temperature profile also affects the polymer viscosity profile and viscosity build-up.

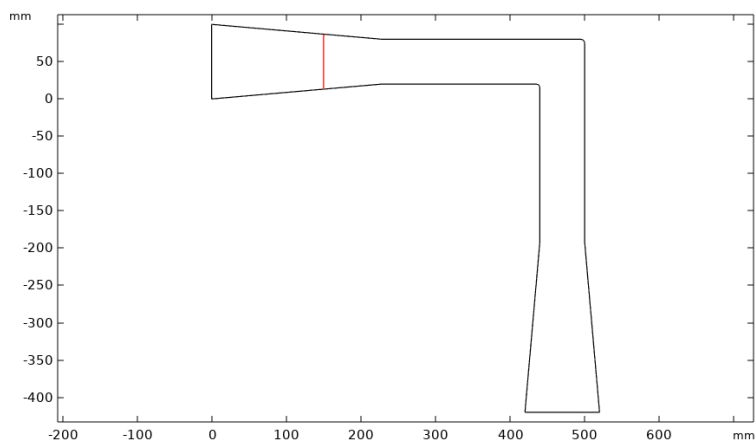


Figure 24 . Polymer Temperature Profile Location

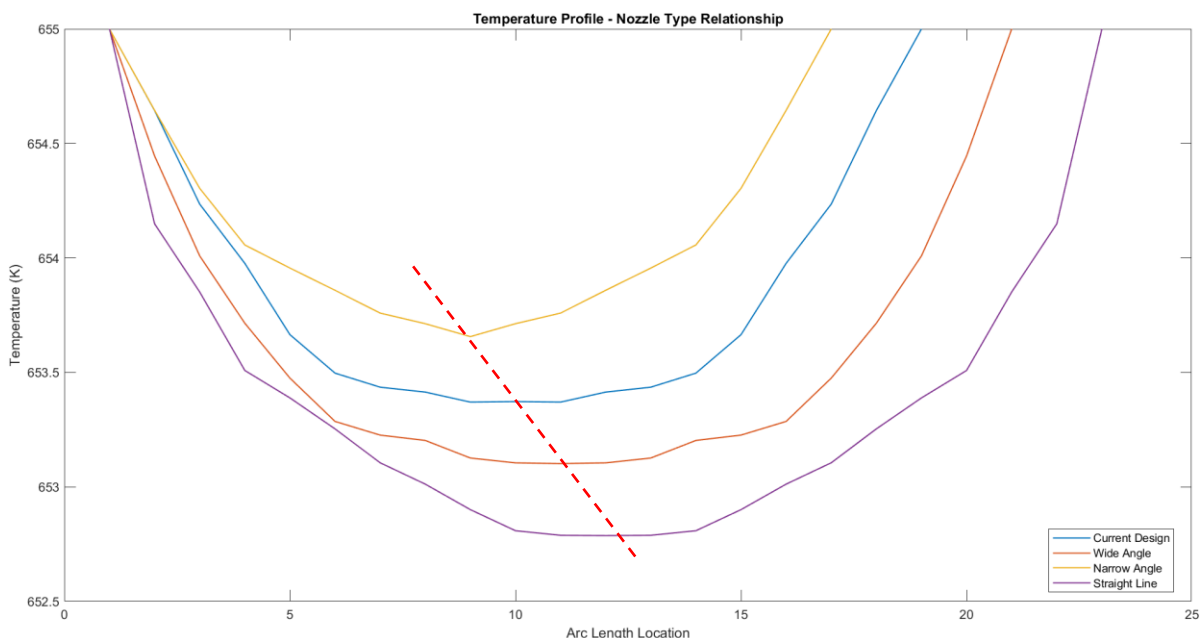


Figure 25 . Polymer Temperature Profile for 4 Nozzle Designs

After examining the relationship between nozzle design and temperature distribution, it was determined how the temperature distribution affected the polymer in terms of reaction and temperature. Although the temperature condition on the pipe walls is the same in all nozzle designs, the temperature distribution of the polymer varies due to the contraction of the pipe. The changing temperature profile directly affects the reaction rate and the molecular weights of the polymer chains formed accordingly. This weight difference was calculated using the experimental viscosity values defined in Comsol, which were also described in the previous sections of this thesis. Because the center is exposed to more temperature than the other nozzle

designs in the narrow-angle nozzle model, where a sudden temperature increase is observed, the polymer center viscosity value is higher in this nozzle model than in the other nozzle designs. While the lowest viscosity value in the center is observed in the straight pipeline, this viscosity value is followed by the wide-angle nozzle design and the existing design, respectively. Following the calculations, as seen in the graph, sudden diameter contractions on the polymer line result in temperature increases inside the polymeric fluid. These temperature increases directly impact the chemical reaction and the profile of viscosity build-up. Temperature increases in the polymer core might cause cross-linking, which enhances the likelihood of gel formation in the polymer center. In order to reduce the probability of gel formation, it is important to ensure that the temperature is uniformly distributed linearly down the line, preventing unexpected temperature increases. As can be seen in the figure (32), in the narrow angle nozzle design the central point of the polymeric fluid reaches the highest temperature, which creates the highest probability of gel formation among these four nozzles. Straight line design, in which the temperature does not increase non-uniformly, has the lowest chance of cross-linking since there is no non-uniform temperature rise in the core of the polymeric fluid and the rate of gel formation is minimal, resulting in the lowest probability of cross-linking.

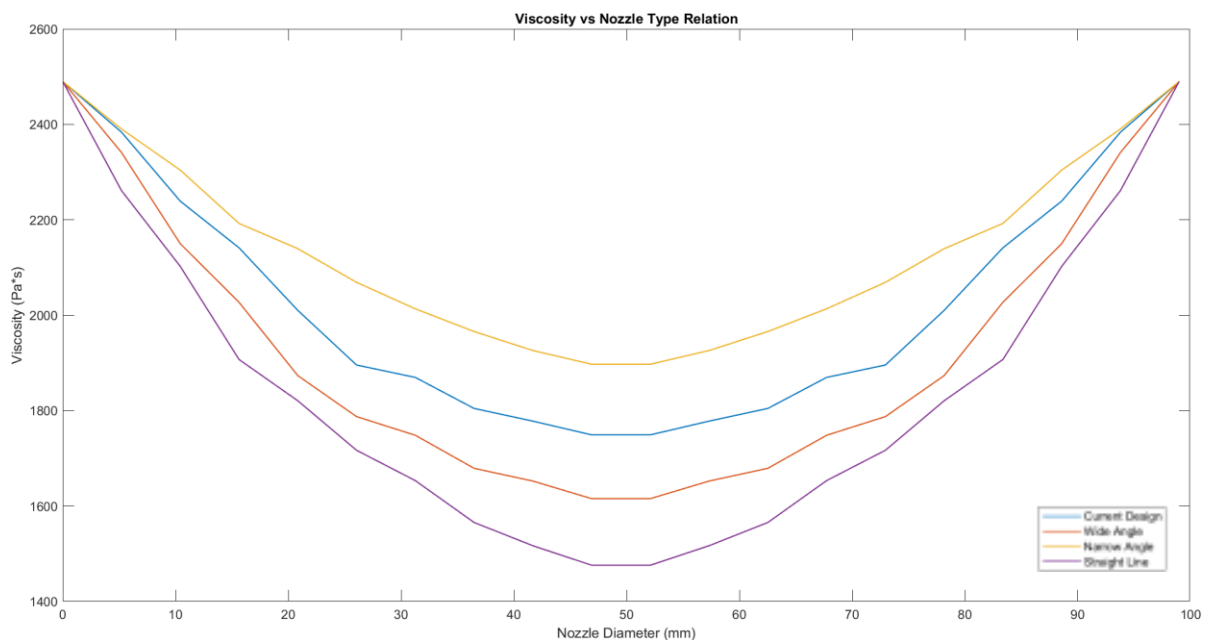


Figure 26 . Viscosity Distribution Profile for Four Nozzle Designs Along the Pipe Diameter

Because of the narrowing in diameter of the line, the rate of heat transfer changes, and the resulting change in heat transfer rate affects the temperature distribution of the polymer as well. The different temperature distributions formed between the wall and the center directly impacted the profile of polymer viscosity build-up in the direction of the polymeric fluid. Because of the higher central polymer temperature, it is observed that the narrow-angle nozzle design, which has a viscosity difference of approximately 125 Pa*s between the entry and exit points, has the maximum reaction rate depending on the viscosities at the inlet and the outlet points. The wide-angle nozzle design and the straight pipeline design both show a slower reaction rate with viscosity differences of 75 Pa*s and 85 Pa*s, respectively. Because the temperature and inlet boundary conditions are the same, the local change throughout the viscosity build-up profile also affects the viscosity build-up profile within the line, resulting in different reaction dynamics at different points which interrupts the homogeneity. This can impact the computation of the target viscosity value of the whole polymerization line and increase the probability of gel formation by locally forming cross-links at the points where the temperature and reaction rate suddenly. According to figure (33), in the narrow-angle nozzle design, the increased reaction rate with the effect of heat transfer accelerated the viscosity increase. For this reason, the viscosity increase rate is observed the most in narrow-angle nozzle design and the least in straight pipeline.

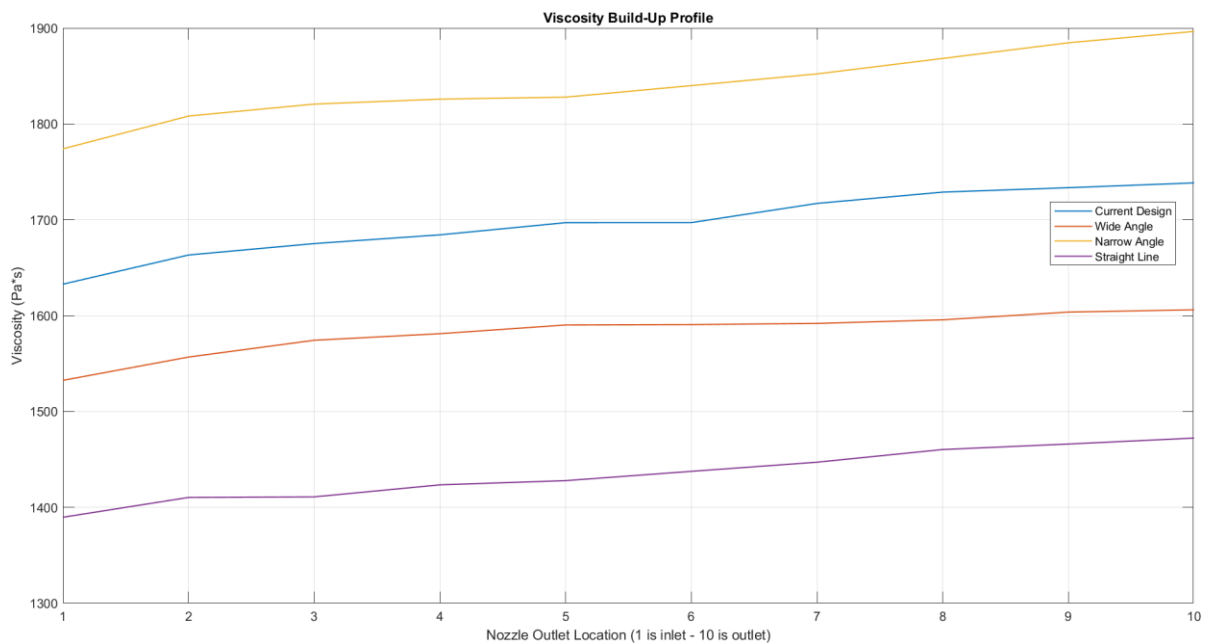


Figure 27 . Viscosity Build-up Profile for 4 Nozzle Designs Along the Pipe Diameter

CHAPTER 6

CONCLUSION

In this thesis, the effects of nozzle geometry on the temperature distribution and reaction rate in the polymeric flow were investigated. To investigate the geometrical effects, all other boundary conditions are kept constant. The effect of each nozzle design on the viscosity build-up profile was determined by comparing the viscosity values in the COMSOL program. The viscosity build-up profile is also closely related with the cross-linking occurrence in the polyamide 66 polycondensation process. Cross-linking in polymers is occurred mostly because of rapid temperature increases and continuous exposure to high temperatures. After the relevant governing equations describing the physics in this problem are solved by using the Comsol program, four different flow analysis were obtained depending on the nozzle type. According to the flow analysis, it is possible to heat the polymer in the center of the line only by narrowing the line diameter; nevertheless, the reaction dynamics change due to this heating. The lowest viscosity and the reaction rate are obtained in the straight-line nozzle design, where the polymer temperature is distributed uniformly. In this nozzle design, no sudden temperature increases, or high temperature exposure is observed within the polymeric fluid domain. Therefore, compared to other nozzle designs, this nozzle design has the lowest possibility of cross-linking and gelation. On the other hand, the narrow-angle nozzle design has the greatest center polymer temperature. Compared to other nozzle designs, this nozzle design has the highest probability of cross-linking and gel formation due to the rapid heating and high temperature exposure. In the polymerization lines, these contractions directly affect the viscosity distribution and viscosity build-up profiles. As a result, these reductions on the polymerization line should be avoided, since it affects the viscosity build up profile and viscosity distribution homogeneity, and when it is necessary to put reductions in this manner, the transition should be made as smooth as possible in terms of diameter decrease. As the pipe diameter reduction increases, the probability of rapid heating and high-temperature exposure also increases, therefore, the probability of cross-linking and non-uniform viscosity build up in the polymer also increases. Straight pipeline dimensions should be maintained throughout the polymerization line for the reaction to proceed as homogeneously as possible in terms of viscosity. The nozzles' type on the line directly affects the temperature distribution of the polymer and the profile of viscosity build-up. The reaction rate increases as the temperature of the core polymer increases.

FUTURE WORKS

In Kordsa polymerization line, current nozzle type is used. In order to have a more uniform viscosity distribution and temperature profile inside the polymerization line straight line or wide-angle nozzle design can be used. Optimization of the Kordsa Continuous Polymerization Line is considered for future works.

Also, COMSOL reacting flow model will be applied for the other production lines. Optimization studies will be carried out for other polymerization lines of Kordsa.

In this thesis, the chemical reacting flow model was created by experimental data. In the future studies, this chemical reacting flow model will be created by using the polymerization equations in order to calculate the molarity change of the products. By this way, this model can be applied to any other polymerization line without the need of experimental data.

REFERENCES

1. Kohan, M. I. (1995). *Nylon plastics handbook*. Hanser.
2. Bievre, B. D. (2000). Polyamide 2000 World Congress. Zurich; Maack Business Services.
3. Charaf, F. (2000). Polyamide 2000 World Congress. Zurich; Maack Business Services.
4. Palmer, R.J. (2001). Polyamides, Plastics. In *Encyclopedia of Polymer Science and Technology*, (Ed.). <https://doi.org/10.1002/0471440264.pst251>
5. Lewin, M., Pearce, E. M. (1998). *Handbook of Fiber Chemistry* (3rd ed.). Marcel Dekker.
6. Carothers W.H. (to E I du Pont de Nemours & Co., Inc.). (1937). Linear condensation polymers (2 071 250). US Patent Office.
7. Carothers W.H. (to E I du Pont de Nemours & Co., Inc.). (1937). Linear condensation polymers (2 071 253). US Patent Office.
8. Carothers W.H. (to E I du Pont de Nemours & Co., Inc.). (1938). Linear condensation polymers (2 130 523). US Patent Office.
9. Carothers W.H. (to E I du Pont de Nemours & Co., Inc.). (1938). Linear condensation polymers (2 130 948). US Patent Office.
10. Deopura, B. L., Alagirusamy, R., Joshi, M., & Gupta, B. (2008). *Polyesters and Polyamides* (Woodhead Publishing Series in Textiles) (1st ed.). Woodhead Publishing.
11. McIntyre, J. E. (2005). Nylon fibres. In *Synthetic fibres: Nylon, polyester, acrylic, polyolefin*. essay, Woodhead Publishing.
12. Mark, H. F. (2004). *Encyclopedia of Polymer Science and Technology, Part 3 (ENCYCLOPEDIA OF POLYMER SCIENCE AND ENGINEERING 3RD EDITION) (Volumes 9–12)* (Volumes 9–12 ed., Vol. 11). Wiley-Interscience.
13. Stepan, D. D., Doherty, M. F., & Malone, M. F. (1987). A kinetic and equilibrium model for nylon 6,6 polymerization. *Journal of Applied Polymer Science*, 34(6). <https://doi.org/10.1002/app.1987.070340624>
14. Hougen, O. A., Ragatz, R. A., Watson, K. M. (2004). *Chemical process principles*. Wiley.
15. Smith, J. M., C., V. N. H. (1981). *Introduction to chemical engineering thermodynamics*. McGraw-Hill Int. Book Co.

16. Wiloth, F. (1955). Makromol. Chem., 15(1), 98–105. <https://doi.org/10.1002/macp.1955.020150109>
17. Ogata, N. (1961). Makromol. Chem., 43(1), 117–131. <https://doi.org/10.1002/macp.1961.020430111>
18. Giori, C., Hayes, B. T. (1970). Journal of Polymer Science Part A-1: Polymer Chemistry, 8(2), 355. <https://doi.org/10.1002/pol.1970.150080207>
19. Zimmerman, J., Jacobs, D. B. (1977). Preparation of 6,6-Nylon and Related Polyamides. In C. E. Schildknecht; I. Skeist (Eds.), Polymerization Processes., Wiley.
20. David, C. (1975). Chapter 1 thermal degradation of polymers. Degradation of Polymers, 1–173. [https://doi.org/10.1016/s0069-8040\(08\)70333-9](https://doi.org/10.1016/s0069-8040(08)70333-9)
21. Pilati, F. (1989). Solid-state polymerization. Comprehensive Polymer Science and Supplements, 201–216. <https://doi.org/10.1016/b978-0-08-096701-1.00154-3>
22. Schaffer, M. A., McAuley, K. B., Marchildon, E. K., Cunningham, M. F. (2007). Thermal degradation kinetics of Nylon 66: Experimental study and comparison with model predictions. Macromolecular Reaction Engineering, 1(5), 563–577. <https://doi.org/10.1002/mren.200700020>
23. Yang, R. (2020). Polymer degradation and stability. Polymer Science and Nanotechnology, 125–148. <https://doi.org/10.1016/b978-0-12-816806-6.00007-8>
24. Peebles, L. H., Huffman, M. W. (1971). Thermal degradation of nylon 66. Journal of Polymer Science Part A-1: Polymer Chemistry, 9(7), 1807–1822. <https://doi.org/10.1002/pol.1971.150090703>
25. Flory, P. J. (1954). Principles of polymer chemistry. Cornell University Press.
26. Flory, P. J. (1936). Molecular size distribution in linear condensation polymers. Journal of the American Chemical Society, 58(10), 1877–1885. <https://doi.org/10.1021/ja01301a016>
27. Tobita, H., Ohtani, Y. (1992). Control of molecular weight distribution in step-growth polymerization: The intermediate monomer feed method. Polymer, 33(4), 801–811. [https://doi.org/10.1016/0032-3861\(92\)90340-3](https://doi.org/10.1016/0032-3861(92)90340-3)
28. Huggins, M. L. (1942). The viscosity of dilute solutions of long-chain molecules. iv. dependence on concentration. Journal of the American Chemical Society, 64(11), 2716–2718. <https://doi.org/10.1021/ja01263a056>
29. Kraemer, E. O. (1938). Molecular weights of celluloses and cellulose derivatives. Industrial; Engineering Chemistry, 30(10), 1200–1203. <https://doi.org/10.1021/ie50346a023>

30. Vulterin, J. (1966). Ferrimetrische Perjodatbestimmung. Collection of Czechoslovak Chemical Communications, 31(9), 3529–3535. <https://doi.org/10.1135/cccc19663529>
31. Lánská, B., Bohdanecký, M., Šebenda, J., Tuzar, Z. (1978). Dilute solutions of Nylon 12—II. relationship between intrinsic viscosity and molecular weight. European Polymer Journal, 14(10), 807–810. [https://doi.org/10.1016/0014-3057\(78\)90178-7](https://doi.org/10.1016/0014-3057(78)90178-7)
32. Morgan, P. W., Kwolek, S. L. (1963). Interfacial polycondensation. XIII. viscosity–molecular weight relationship and some molecular characteristics of 6-10 polyamide. Journal of Polymer Science Part A: General Papers, 1(4), 1147–1162. <https://doi.org/10.1002/pol.1963.100010407>
33. Tuzar, Z., Kletečková, J., Králíček, J. (1974). Properties of dilute polypyrolidone solutions. Collection of Czechoslovak Chemical Communications, 39(8), 2206–2211. <https://doi.org/10.1135/cccc19742206>
34. Reimschuessel, H. K., Dege, G. J. (1971). On the condensation equilibrium in the polymerization of caprolactam. Journal of Polymer Science Part A-1: Polymer Chemistry, 9(8), 2343–2359. <https://doi.org/10.1002/pol.1971.150090821>
35. Tuzar, Z., Kratochvíl, P. (1967). Light scattering. XVIII. the behaviour of polymers in mixed solvents. Collection of Czechoslovak Chemical Communications, 32(9), 3358–3370. <https://doi.org/10.1135/cccc19673358>
36. Goebel, C. V., Čefelín, P., Stehlíček, J., Šebenda, J. (1972). Anionic polymerization of caprolactam. XLIII. relationship between osmometric molecular weight, viscosity, and end groups of a polymer. Journal of Polymer Science Part A-1: Polymer Chemistry, 10(5), 1411–1427. <https://doi.org/10.1002/pol.1972.150100512>
37. Schaefgen, J. R., Flory, P. J. (1948). Synthesis of multichain polymers and investigation of their viscosities. Journal of the American Chemical Society, 70(8), 2709–2718. <https://doi.org/10.1021/ja01188a026>
38. Gechele, G. B., Mattiussi, A. (1965). Intrinsic viscosity-molecular weight relations for hydrolytic polycaprolactam. European Polymer Journal, 1(1), 47–61. [https://doi.org/10.1016/0014-3057\(65\)90046-7](https://doi.org/10.1016/0014-3057(65)90046-7)
39. Burke, J. J., Orofino, T. A. (1969). Nylon 66 polymers. I. Molecular Weight and compositional distribution. Journal of Polymer Science Part A-2: Polymer Physics, 7(1), 1–25. <https://doi.org/10.1002/pol.1969.160070101>
40. von Elias, H.-G., Schumacher, R. (1964). Über das Lösungsverhalten von Nylon 6,6. Die Makromolekulare Chemie, 76(1), 23–53. <https://doi.org/10.1002/macp.1964.020760103>

41. Taylor, G. B. (1947). The relation of the viscosity of nylon solutions in formic acid to molecular weight as determined by end-group measurements. *Journal of the American Chemical Society*, 69(3), 635–638. <https://doi.org/10.1021/ja01195a050>
42. Liquori, A. M., Mele, A. (1954). Viscous behavior of polyhexamethylenadipamide molecules in solution. *Journal of Polymer Science*, 13(72), 589–594. <https://doi.org/10.1002/pol.1954.120137209>
43. Burke, J. J., Orofino, T. A. (1969). Nylon 66 polymers. I. Molecular Weight and compositional distribution. *Journal of Polymer Science Part A-2: Polymer Physics*, 7(1), 1–25. <https://doi.org/10.1002/pol.1969.160070101>
44. Ease, M., Barigou, M. (2009). CFD investigation of the pipe transport of coarse solids in laminar power-law fluids. *Chemical Engineering Science*, 64(2), 322–333. <https://doi.org/10.1016/j.ces.2008.10.004>
45. Chabra, R.P., Richardson, J.F., 1985. Hydraulic transport of coarse particles in viscous Newtonian and non-Newtonian media in a horizontal pipe. *Chemical Engineering Research & Design* 63, 390–397.